AD-A058 088 FLIGHT DYNAMICS RESEARCH CORP VAN NUYS CALIF F/G 13/10.1
UNDERWATER JET-DIFFUSER EJECTOR PROPULSION. REAL FLUID EFFECTS.(U)
AUG 78 M ALPERIN, J WU N00014-77-C-0294
UNCLASSIFIED FDRC-0294-8-78 NL

END
DATE FILMED
10-78
DDC

LEVEL II

FDRC 0294-8-78

12

UNDERWATER JET-DIFFUSER EJECTOR PROPULSION
REAL FLUID EFFECTS

by
MORTON ALPERIN and JIUNN-JENQ WU

August 1978

Sponsored by
Office of Naval Research
Contract No. N00014-77-C-0294

FLIGHT DYNAMICS RESEARCH CORPORATION
VAN NUYS, CALIFORNIA 91406

(9) Final rept. 1 Apr 77 - 31 Jul 78,

UNCLASSIFIED

SECURITY CLASSIFICATION OF THIS PAGE (When Data Entered)

REPORT DOCUMENTATION PAGE

READ INSTRUCTIONS BEFORE COMPLETING FORM

1. REPORT NUMBER: FDRC-0294-8-78

2. GOVT ACCESSION NO.

3. RECIPIENT'S CATALOG NUMBER

4. TITLE (and Subtitle) (6): UNDERWATER JET-DIFFUSER EJECTOR PROPULSION, REAL FLUID EFFECTS,

5. TYPE OF REPORT & PERIOD COVERED: FINAL REPORT, 1 Apr '77 through 31 July '78

6. PERFORMING ORG. REPORT NUMBER (14): FDRC-0294-8-78

7. AUTHOR(s) (10): Morton Alperin and Jiunn-Jeng Wu

8. CONTRACT OR GRANT NUMBER(s) (15): N00014-77-C-0294

9. PERFORMING ORGANIZATION NAME AND ADDRESS:
Flight Dynamics Research Corporation
15809 Stagg Street
Van Nuys, Ca. 91406

10. PROGRAM ELEMENT, PROJECT, TASK AREA & WORK UNIT NUMBERS:
Program Element 61153N
Project RRO 24-03-02
Work Unit NR 097-411

11. CONTROLLING OFFICE NAME AND ADDRESS:
Office of Naval Research
800 North Quincy Street
Arlington, Va. 22217

12. REPORT DATE (11): August 1978

13. NUMBER OF PAGES (12): 96 pp.

14. MONITORING AGENCY NAME & ADDRESS (if different from Controlling Office) (16) RRO 2403 (17) RRO 240302:
SAME AS BLOCK 11

15. SECURITY CLASS. (of this report): UNCLASSIFIED

15a. DECLASSIFICATION/DOWNGRADING SCHEDULE

16. DISTRIBUTION STATEMENT (of this Report)

Approved for public release; Distribution unlimited

17. DISTRIBUTION STATEMENT (of the abstract entered in Block 20, if different from Report)

SAME AS BLOCK 16

18. SUPPLEMENTARY NOTES

19. KEY WORDS (Continue on reverse side if necessary and identify by block number)

Ejector
Propulsion
Thrust Augmentation
Jet-Diffuser
Mixing

20. ABSTRACT (Continue on reverse side if necessary and identify by block number)

SEE BACK OF FORM

405018

DD FORM 1 JAN 73 1473 EDITION OF 1 NOV 65 IS OBSOLETE
S/N 0102-LF-014-6601

UNCLASSIFIED
SECURITY CLASSIFICATION OF THIS PAGE (When Data Entered)

20. Abstract

The flow properties and performance of a jet-diffuser and a conventional ejector in an underwater environment, including the influence of losses due to inlet blockage, skin friction, incomplete mixing, diffuser separation and nozzle efficiency have been determined. Analytical methods for the evaluation of the loss coefficients from experiments are described.

The importance of a proper selection of pump characteristics to optimize the performance of ejectors of any given geometric size are discussed and some examples of the optimization procedure are presented.

The influence of performance limitations due to cavitation, viscous dissipation and self-propulsion are discussed with some specific examples which illustrate these limitations as applied to the performance of ejectors with realistic losses.

FDRC 0294-8-78

UNDERWATER JET-DIFFUSER EJECTOR PROPULSION
REAL FLUID EFFECTS

by
MORTON ALPERIN and JIUNN-JENQ WU

August 1978

Sponsored by
Office of Naval Research
Contract No. N00014-77-C-0294

FLIGHT DYNAMICS RESEARCH CORPORATION
VAN NUYS, CALIFORNIA 91406

PREFACE

The effort reported in this document was performed by Flight Dynamics Research Corporation during the period April 1977 through July 1978. The sponsorship was provided by the Office of Naval Research, Arlington Va. under Contract No. N00014-77-C-0294. Technical coordination was provided by Mr. Keith Ellingsworth, Scientific Officer, Power Programs, of the Office of Naval Research.

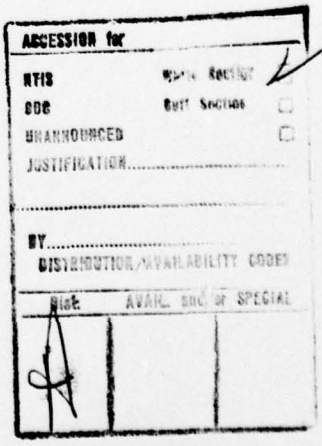

SUMMARY

The performance of an ejector whose only loss is that of the intrinsic energy dissipation due to mixing is shown to be a function of the dimensionless ratio of free-stream dynamic pressure to the pump head ($q_\infty/\Delta P$). Increasing values of this ratio results in a decrease in the thrust augmenting capability of an ideal ejector, when other parameters remain fixed.

An ejector which ingests free-stream fluid is shown to be subject to performance limitations imposed by cavitation, by the degradation of the diffuser jet due to skin friction and by the limit of self-propulsion (if applicable). Cavitation is a limiting factor for all types of ejectors, depending upon the ratio of throat area to total nozzle area, the diffuser area ratio and the depth and speed of the vehicle. The limit due to skin friction at the interface of the diffuser jet and the solid diffuser surface occurs only in jet-diffuser ejectors and can easily be remedied by an increase of the injected momentum of the diffuser jet fluid. The limit of self-propulsion occurs when the effluent flow has a mass averaged velocity equal to the free-stream velocity. Ingestion of boundary layer fluid is shown to result in large performance gains, but the limit of self-propulsion is somewhat more severe due to the requirement for larger momentum increments.

The relatively small length of a jet-diffuser compared to a more conventional solid diffuser has raised questions regarding the feasibility of achieving adequate mixing of primary and induced flows. A jet-diffuser provides a lengthy region beyond the end of the solid surfaces of the ejector in which effective mixing can occur. In addition however it has been shown that an increase in the effective diffuser area ratio (such as that achieved by a properly designed jet-diffuser) can compensate for the lack of complete mixing. Thus the design of an efficient, short, large area ratio diffuser is more important than the achievement of complete mixing - particularly if the attempt to attain complete mixing involves the introduction of additional losses.

The influence of various losses on ejector performance is discussed and illustrated in terms of some specific examples at speeds of 12.9 m/sec (25 knots) and 25.7 m/sec (50 knots) for both free-stream and boundary layer inlets. Losses due to skin friction are evaluated using classical skin friction laws and empirical loss factors for inlet and nozzle losses.

The achievement of optimal performance from ejector thrusters is shown to depend very strongly upon a proper choice of pump head (ΔP) and diffuser area ratio (δ), to match any given choice of area ratio $A_2/(s_\infty + a_\infty)$, for any given speed, depth and loss coefficients. Examples of the method of optimization are presented for free-stream and for boundary layer inlet conditions and the optimal performance arrived at by this procedure is presented for a range of values of the inlet drag coefficient.

The ratio of diffuser jet mass flow to primary jet mass flow must also be selected for optimal performance and for satisfactory boundary layer control. Data for a selected set of conditions are presented to illustrate the dependance of thrust augmentation on the ratio $\dot{m}_d/\dot{m}_p$. For the conditions used on the illustration, optimal values of this ratio of injected mass flows are between 0.05 and 0.2 at high speed varying with the types of inlet flow, the inlet drag coefficient and the vehicle speed. Optimal values of $\dot{m}_d/\dot{m}_p$ are larger at low speeds.

LIST OF FIGURES

LIST OF FIGURES (Concluded)

LIST OF SYMBOLS

A	duct area
a	primary jet area or thickness
C	coefficient
C_F	coefficient of skin friction (area based on throat)
C_f	coefficient of skin friction (area based on wetted surface)
ε	mechanical energy loss per unit time
F	net thrust
f	force
H	diffuser jet characteristic
ℓ	length
$\dot{m}$	mass flow rate
P	power or stagnation pressure
p	pressure
q	dynamic pressure
R	radius of curvature
Re_ℓ	Reynolds number
R_p	relative power
r	entrainment ratio
S	wetted surface area
s	diffuser jet area or thickness
t	jet thickness
U	secondary or mixed flow velocity
$\overline{U}$	averaged core flow velocity
U'	perturbation velocity
V	jet velocity
V'	jet velocity after lossless expansion from the plenum
X	duct width
$\tilde{X}$	effective duct width
x	coordinate in the thrust direction
y	lateral coordinate

LIST OF SYMBOLS (Concluded)

α	inlet area ratio (= A_2/a)
β	diffuser jet exit angle
δ	geometric diffuser area ratio (= X_3/X_2)
δ^*	effective diffuser area ratio (= $\tilde{X}_3/X_2$)
ζ	combined parameter of static and total pressure surveys
η	propulsive efficiency or efficiency factor
θ	diffuser jet angle with respect to thrust direction
ΔP	pump pressure rise
λ	non-dimensional mean velocity (= $\bar{U}/V_{pl}$)
μ	absolute viscosity
ρ	mass density
σ	effective diffuser area ratio of a jet-diffuser
ϕ	thrust augmentation

Subscripts

c	critical or core flow
d	diffuser duct
di	inlet drag
dj	diffuser jet or jet-diffuser
e	ejector inlet
eff	effective
ej	ejector
i	induced flow
j	jet
N	primary nozzle
m	mixing duct
p	pump inlet or primary jet
ref	reference jet
o	unaugmented or stagnation
T	total
t	stagnation
1,2,3,4,J	ejector stations
∞	undisturbed or ambient condition
μ	non-uniformity

TABLE OF CONTENTS

TABLE OF CONTENTS (Concluded)

I INTRODUCTION

The thrust augmenting capability of ejectors has been known for several decades, but the practical utilization of these devices has been limited by their large size and the drag associated with their integration into vehicle systems. Recent advances in ejector technology and a better understanding of the influence of various controllable properties of the injected and induced flows have provided a basis for large reduction in size and optimization of the performance of these devices.

The large size required by ejectors has been due to the use of conventional type diffusers which require a large area ratio for the recovery of jet kinetic energy. To achieve large area ratios and to avoid separation, conventional diffusers must diverge slowly with a divergence half angle which does not exceed about ten degrees. In addition, to provide sufficient length for mixing of primary and induced fluids, many ejector designs included a region of constant cross-section upstream of the diffuser. The combination of mixing section and solid surface diffusers resulted in excessively long structures thereby causing serious integration and drag problems.

The development of efficient jet-diffusers for ejectors under the U. S. Navy / Marine Corps STAMP (Small Tactical Aerial Mobility Platform) Program, reported in Reference 1, has resulted in a major reduction in the size required for diffusers and has simultaneously extended the region available for mixing.

A jet-diffuser ejector is an ejector which utilizes a high velocity jet located within a rapidly diverging solid diffuser duct to

a) avoid separation despite large diffuser divergence angles;

b) provide a means for increasing the effective diffuser area ratio to values in excess of that of the solid surfaces, and;

c) provide a lengthy region for effective mixing without the need for lengthy solid surfaces.

The resulting performance/size advantage attributable to this concept has been demonstrated under stationary conditions and is reported in Reference 1.

It has been shown in Reference 2 that the use of ejectors for underwater propulsion provides a large performance advantage and a considerable savings in jet power, and therefore a reduction in space requirements for machinery and fuel. That work however did not encompass the use of jet-diffusion.

This document reports an analytical approach, based upon the approximations utilized in jet-flapped wing theory (Reference 3) but with application to the jet-diffuser flow situation. This analysis provides a means for determination of the flow through, and the overall performance of, a translating jet-diffuser and a solid diffuser ejector, including the influence of inlets located in a boundary layer or wake, and various loss factors. Individual loss factors can either be measured or evaluated by methods described and, when utilized in the analysis, can serve as guide for ejector design.

II PHYSICAL CONSIDERATIONS

In the mathematical model, high velocity incompressible fluid issues from the primary jet at Station 1 and for a jet-diffuser the diffuser jet issues at Station J, as illustrated on Figure 1.

The primary fluid which issues at Station 1 is assumed to mix with the captured fluid between Stations 1 and 2, in a duct of constant cross-section.

The diffuser jet fluid injected at Station J is assumed to proceed with a loss due to skin friction, but unmixed with the core flow, past Station 3 (the end of the solid diffuser) to a remote region (Station 4) where all flows are returned to the ambient pressure. At Station 4, the diffuser jet and its external and core flows are in the free stream direction as a consequence of the symmetry of the ejector.

In the analysis which follows, the influence of skin friction and obstacle drag will be considered as a decrement to the momentum flux through each section of the ejector. Thus a correction term equal to the force due to viscosity will be applied to the momentum flux determined by inviscid considerations.

The mathematical treatment will consider first a solid diffuser ejector, then by modification of those equations to include the influence of a jet-diffuser and its losses, the jet-diffuser ejector will be described.

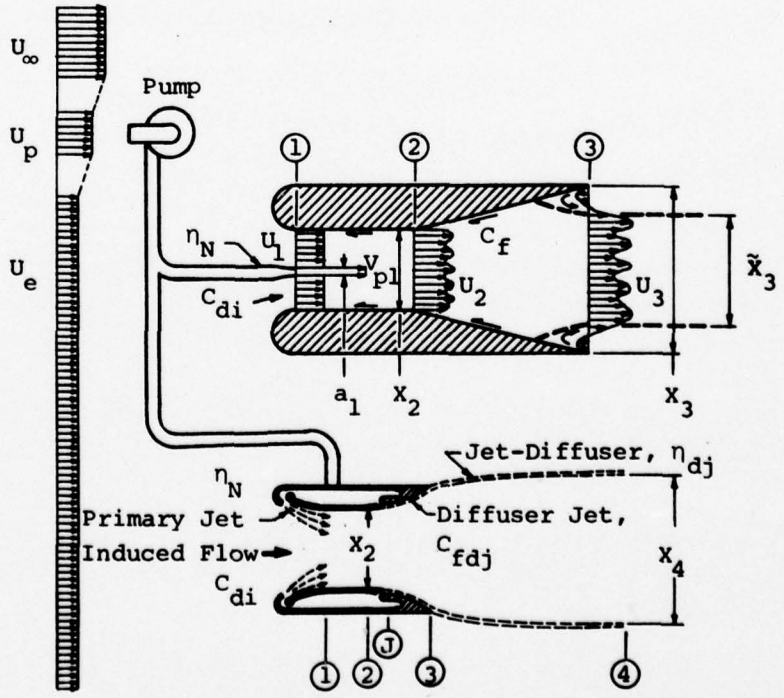

Figure 1. MATHEMATICAL MODEL OF SOLID AND JET-DIFFUSER EJECTORS

III MATHEMATICAL CONSIDERATIONS

1. Solid Diffuser Ejector

a) Basic Theory

The analysis of the flow through a solid diffuser ejector is carried out by application of the laws of mass flow, momentum, and energy conservation through the ejector duct, considering the influence of skin friction as a force in the direction opposite to that of the mean flow. At the inlet of the ejector, the drag of obstacles and the influence of skin friction are considered to be related to the dynamic pressure at the ejector's inlet (Station 1). The influence of this force can be expressed as a loss of stagnation pressure during the ingestion process. Thus,

$$P_{oe} - P_{o1} = C_{di}(\rho/2)U_1^2 \tag{1}$$

which then translates into the Bernoulli Equation as

$$p_1 - p_\infty = (\rho/2)U_e^2 - (\rho/2)U_1^2(1 + C_{di}) \tag{2}$$

Adopting the notation λ_k ($= \bar{U}_k/V_{pl}$) to non-dimensionalize the local mean velocities, Equation 2 reduces to the form

$$p_1 - p_\infty = (\rho/2)V_{pl}^2\{\lambda_e^2 - (1 + C_{di})\lambda_1^2\} \tag{3}$$

The law of mass flow conservation can be stated for the entire flow through the ejector by a series of equations as

$$X_1U_1 + a_1V_{pl} = X_2\bar{U}_2 = \tilde{X}_3\bar{U}_3 \tag{4}$$

where $\tilde{X}_3$ refers to the effective cross-section at Station 3. Thus, the region of separated flow (if any) is not included in the effective cross-section.

In terms of λ, this reduces to the form

$$1 + (\alpha - 1)\lambda_1 = \alpha\lambda_2 = \alpha\delta^*\lambda_3 \tag{5}$$

where

$$\delta^* = \tilde{X}_3/X_2 \quad \text{and} \quad \alpha = X_2/a_1 \tag{6}$$

Mixing is an essential process in the ejector flow. It is well known that loss of mechanical energy occurs during the mixing process. The goal of an ideal ejector is to achieve complete mixing before the end of the ejector flow process. Complete mixing will be accompanied by a maximum mechanical energy loss, but will produce a maximum thrust increment, which is a consequence of increased mass flow. Instead of relying on empirical loss factors, this type of mixing loss can be described accurately by applying conservation laws of mass and momentum flux in the mixing duct. Two types of mixing ducts are commonly used for the analytical treatment, constant area and constant pressure mixing, constant area mixing is adopted in this report.

In order to isolate the mixing loss from other nonessential loss, such as frictional loss, and to provide a means for evaluation of the effect of incomplete mixing as in real ejectors, a fictitious section, (Station 2), is introduced. Flow at Station 2 can be non-uniform (for an ideal ejector, flow is uniform in Station 2) but is assumed to be at its final state of mixing, so that no further energy dissipation due to the essential mixing process occurs downstream of Station 2. Thus, since U_2 is not uniform, the momentum equation must be written as follows.

Momentum (for a constant cross-section)

$$\rho a_1 V_{p1}^2 + \rho U_1^2 (X_2 - a_1) + p_1 X_2 = \int_{X_2} \rho U_2^2 dX_2 + p_2 X_2 + f_m \tag{7}$$

where f_m = Force due to skin friction in the mixing duct (2-dimensional).

If ℓ_m = Length of mixing duct

and C_{fm} = Coefficient of skin friction in the mixing duct,

then

$$f_m = (\rho/2)\bar{U}_2^2 C_{fm}(2\ell_m) \tag{8}$$

If the velocity at Station 2 is expressed as

$$U_2 = \bar{U}_2 + U_2' \tag{9}$$

where $$\bar{U}_2 = (1/X_2)\int_{X_2} U_2 dX_2$$

then upon integration of Equation 7,

$$p_2 - p_1 = \rho V_{p1}^2 \{(1/\alpha) + [(\alpha - 1)/\alpha]\lambda_1^2 - [1 + C_{fm}(\ell_m/X_2) + (\overline{U_2'^2}/\bar{U}_2^2)]\lambda_2^2\} \tag{10}$$

If the diffuser is solid (does not include a diffuser jet), then the pressure at Station 3 must be ambient (p_∞). If the mixing is assumed to remain at the state of completion achieved at Station 2, then no further energy dissipation due to mixing occurs between Stations 2 and 3. Further, if the secondary flow phenomenon (usually encountered in curved diffusers) within the core flow is negligible, the skin friction at the wall and the shear stress on the separated flow (if the flow separates), must be the main mechanism for energy loss in the diffuser.

Assume the total equivalent force due to shear stress and other dissipation mechanisms (if any) in the diffuser is f_d, the mechanical energy loss per unit time (ε) can be expressed as

$$\varepsilon = f_d \bar{U} \tag{11}$$

where $\bar{U}$ is a characteristic velocity. This suggests that the energy loss per unit time can be expressed in terms of a coefficient of friction (C_{fd}) as

$$\varepsilon = (\rho/2)\bar{U}_2^3 C_{fd} S_d \tag{12}$$

where S_d is the duct surface area, and C_{fd} is a dimensionless coefficient.

In the two-dimensional case,

$$S_d = 2\ell_d \tag{13}$$

where ℓ_d is the length of the diffuser surfaces in the flow direction.

Therefore

$$\varepsilon = (\rho/2)\bar{U}_2^3 C_{fd} (2\ell_d/X_2) X_2$$

or

$$\varepsilon = (1/2)\bar{U}_2^2 C_{fd} (2\ell_d/X_2) \dot{m}_c \tag{14}$$

where $\dot{m}_c$ is the mass flow in the diffuser, or core flow.

In the event of a non-uniform distribution of the energy, across the ejector's cross-section, the conservation of mechanical energy between Stations 2 and 3 must take the form

$$\int [(p_2/\rho) + U_2^2/2] d\dot{m}_c = \int [(p_\infty/\rho) + U_3^2/2] d\dot{m}_c + \varepsilon \tag{15}$$

Since p_2 and p_∞ are constants, and for every stream tube,

$$d\dot{m}_c = \rho U_2 dX_2 = \rho U_3 dX_3 \tag{16}$$

and if the velocity distributions are described as

$$U_k = \bar{U}_k + U'_k \qquad (k = 2, 3) \tag{17}$$

where

$$\bar{U}_k = (1/X_k) \int U_k dX_k \tag{18}$$

then after integration, Equation 15 takes the form,

$$\frac{(p_\infty - p_2)}{(\rho/2)V_{p1}^2} = \{1 + 3(\overline{U_2'^2}/\bar{U}_2^2) + (\overline{U_2'^3}/\bar{U}_2^3) - (1/\delta^*)^2 [3(\overline{U_3'^2}/\bar{U}_3^2) + (\overline{U_3'^3}/\bar{U}_3^3)] - 2C_{fd}(\ell_d/X_2)\}\lambda_2^2 - \lambda_3^2 \tag{19}$$

Combination of this equation with Equations 3, 5, and 10 provides the result

$$\lambda_3^2 = \lambda_e^2 + [(1-\lambda_1^2)/\alpha^2] \left[1 + \frac{2(\alpha - 1)}{1 + \lambda_1}\right] - C_{di}\lambda_1^2 - \left[\frac{1+(\alpha - 1)\lambda_1}{\alpha}\right]^2 [C_F + C_\mu] \tag{20}$$

where the loss coefficient due to shear stress (C_F) contains the terms

$$C_F = 2C_{fm}(\ell_m/X_2) + 2C_{fd}(\ell_d/X_2) = 2C_f(\ell_T/X_2) \tag{21}$$

where $\ell_T = \ell_m + \ell_d$ = total ejector length after injection, and the loss coefficient due to non-uniformity (C_μ) contains the terms

$$C_\mu = (1/\delta^*)^2 [3(\overline{U_3'^2}/\bar{U}_3^2) + (\overline{U_3'^3}/\bar{U}_3^3)] - [(\overline{U_2'^2}/\bar{U}_2^2) + \overline{U_2'^3}/\bar{U}_2^3)] \tag{22}$$

Typical survey at the throat section of jet-diffuser ejectors, where the mixing process is far from complete, indicates that $\overline{u'^2}/\bar{u}^2$ is about 0.01, and $\overline{u'^3}/\bar{u}^3$ is about 0.0001, or

$$(\overline{u'^3}/\bar{u}^3) \ll (\overline{u'^2}/\bar{u}^2) \ll 1$$

Therefore, C_μ can be approximated by,

$$C_\mu = (1/\delta^{*2}) \{2(\overline{u'^2_3}/\bar{u}^2_3) + [(\overline{u'^2_3}/\bar{u}^2_3) - \delta^{*2}(\overline{u'^2_2}/\bar{u}^2_2)]\}$$

Further assume,

$$(\overline{u'^2_3}/\bar{u}^2_3) \gg [(\overline{u'^2_3}/\bar{u}^2_3) - \delta^{*2}(\overline{u'^2_2}/\bar{u}^2_2)]$$

since the right hand side of the equation is zero when $\delta^* = 1$ (where Section 2 and Section 3 are coincident). Therefore, only the leading term for C_μ is predominant and

$$C_\mu \cong (2/\delta^{*2})(\overline{u'^2_3}/\bar{u}^2_3)$$

Using this expression for C_μ and noting that for small values of $(\overline{u'^2_3}/\bar{u}^2_3)$,

$$1 + 2(\overline{u'^2_3}/\bar{u}^2_3) \cong [1 + (\overline{u'^2_3}/\bar{u}^2_3)]^2$$

Equation 20 can be rewritten as

$$\{\lambda_3[1+(\overline{u'^2_3}/\bar{u}^2_3)]\}^2 = \lambda_e^2 + \frac{1-\lambda_1^2}{\alpha^2}\left[1+\frac{2(\alpha-1)}{1+\lambda_1}\right] - C_{di}\lambda_1^2 - C_F\left[\frac{1+(\alpha-1)\lambda_1}{\alpha}\right]^2 \qquad (23)$$

For large α, the contribution of the inlet drag coefficient C_{di} to the loss of λ_3 is similar to that of C_F. Therefore, a low drag inlet is essential for high ejector performance.

It is important to note here that the value of $(\overline{u'^2_3}/\bar{u}^2_3)$ depends upon the velocity distribution in the unseparated flow at the diffuser exit and does not include the region of separated flow.

The influence of separation is accounted for in the fact that $\delta \neq \delta^*$. The effective diffuser area ratio $\delta^* = \tilde{X}_3/X_2$ is determined by continuity (Equation 5) and since $\tilde{X}_3$ does not include the separated region of flow, $\tilde{X}_3 \leq X_3$ and $\delta^* \leq \delta$, for a solid diffuser design.

b) Solution of the Solid-Diffuser Ejector Problem

The solid diffuser ejector flow can be uniquely described by Equations 5 and 23, for any given set of parameters describing the ejector geometry, operational conditions, properties of the injected fluid, and the loss coefficients.

Define the primary nozzle thrust efficiency as

$$\eta_N = V_{p\infty}/V'_{p\infty} \tag{24}$$

where,

$V_{p\infty}$ = Primary jet velocity at ambient pressure (with loss)

$V'_{p\infty}$ = Primary jet velocity after a lossless expansion from its stagnation pressure to ambient pressure

Since Bernoulli's Equation for the flow through the pump is

$$(\rho/2)V'^2_{p\infty} = q_p + \Delta P \tag{25}$$

therefore

$$(\rho/2)V^2_{p\infty} = \eta_N^2(q_p + \Delta P) \tag{26}$$

and the Bernoulli's Equation for the primary flow is

$$p_\infty + \eta_N^2(q_p + \Delta P) = p_1 + (\rho/2)V^2_{p1} \tag{27}$$

the expression for λ_e in terms of q_e, and ΔP_{eff}, can be derived by eliminating $(p_\infty - p_1)$ with the use of Equation 3. Thus,

$$(\rho/2)V^2_{p1} = \Delta P_{eff}/[1 - (1 + C_{di})\lambda_1^2] \tag{28}$$

and therefore,

$$\lambda_e^2 = [1 - (1 + C_{di})\lambda_1^2]q_e/\Delta P_{eff} \tag{29}$$

where

$$\Delta P_{eff} = \eta_N^2(\Delta P + q_p) - q_e \tag{30}$$

Substitution of Equation 29 into Equation 23 results in the expression

$$\left\{\lambda_3\left[1+\frac{\overline{U_3'^2}}{\bar{U}_3^2}\right]\right\}^2 = \frac{1-\lambda_1^2}{\alpha^2}\left[1+\frac{2(\alpha-1)}{1+\lambda_1}\right]+[1-(1+C_{di})\lambda_1^2]q_e/\Delta P_{eff}-C_{di}\lambda_1^2-C_F\left\{\frac{1+(\alpha-1)\lambda_1}{\alpha}\right\}^2 \quad (31)$$

Using Equation 5 to express λ_3 in terms of λ_1 provides a quadratic equation in λ_1, where the coefficients are composed of the geometric, operational and injected fluid or pump characteristics, and the quantity $\delta^*/[1 + (\overline{U_3'^2}/\bar{U}_3^2)]$.

Evaluation of the term $\delta^*/[1 + (\overline{U_3'^2}/\bar{U}_3^2)]$ can be accomplished from ejector experiments, as discussed in a later section of this document.

Assuming the term $\delta^*/[1 + (\overline{U_3'^2}/\bar{U}_3^2)]$ to be known, the quadratic equation for λ_1 can be written as

$$A\lambda_1^2 + 2B\lambda_1 + C = 0 \quad (32)$$

where

$$A = (\alpha - 1)^2 + D^2 + \alpha^2 D^2\{(1 + C_{di})(q_e/\Delta P_{eff}) + C_{di} + [(\alpha - 1)/\alpha]^2 C_F\} \quad (33)$$

$$B = (\alpha - 1)\{D^2(1 + C_F) + 1\} \quad (34)$$

$$C = 1 - D^2\{(2\alpha - 1) + \alpha^2(q_e/\Delta P_{eff}) - C_F\} \quad (35)$$

$$D = \delta^*/[1 + (\overline{U_3'^2}/\bar{U}_3^2)]$$

and the solution is

$$\lambda_1 = \frac{-B + \sqrt{B^2 - AC}}{A} \quad (36)$$

The second solution to the quadratic is obviously invalid since it leads to negative values of λ_1.

c) Performance of Solid Diffuser Ejector

The basic performance parameter of any ejector is commonly called thrust augmentation (ϕ), a term which is defined here as the ratio of the net thrust of the ejector (F_{ej}) to the net thrust of a fictitious reference jet (F_{ref}) which is a free jet (discharging without loss to ambient pressure) operating at the same power and mass flow as required the ejector's energized flow.

The term net thrust implies that the drag due to the momentum of ingested fluid (ram drag) is subtracted from the total integrated momentum of the jet with respect to coordinates moving with the vehicle.

Since the effluent flux from the ejector is comprised of fluid which, in general, is ingested at two different locations

a) the ejector's inlet

b) the pump inlet

the ram drag applicable to these mass flows, which may have had different velocities at their respective intake locations, must be considered separately.

Thus the total ejector's discharge mass ($\dot{m}_c$) for a solid diffuser ejector is

$$\dot{m}_c = \rho \int U_3 d\tilde{X}_3 = \rho \tilde{X}_3 \bar{U}_3 = \rho a_1 V_{pl} + \rho X_1 U_1 \tag{37}$$

and the net thrust is given by the momentum increment imparted to these mass flows by the ejector, thus

$$F_{ej} = \rho \int U_3^2 d\tilde{X}_3 - \rho a_1 V_{pl} U_p - \rho X_1 U_1 U_e$$

$$= (\rho a_1 V_{pl}^2)\{\alpha\delta^* \lambda_3^2 [1 + (\overline{U_3'^2}/\bar{U}_3^2)] - \lambda_p - (\alpha - 1)\lambda_1 \lambda_e\} \tag{38}$$

or in terms of the jet quantities at ambient pressure condition and eliminating λ_3 by using Equation 5

$$F_{ej} = \rho a_\infty V_{p\infty}^2 \left\{ [1+(\alpha-1)\lambda_1] \left[[1+(\alpha-1)\lambda_1] \left(\frac{1+(\overline{U_3'^2}/\bar{U}_3^2)}{\alpha\delta^*} \right) - \lambda_e \right] - \lambda_p + \lambda_e \right\} \frac{V_{pl}}{V_{p\infty}} \tag{39}$$

Using Equation 29 to express λ_e in terms of $q_e/\Delta P_{eff}$ and the corresponding expression for λ_p, provides the following relationships.

$$\lambda_e^2 = \frac{q_e[1 - (1 + C_{di})\lambda_1^2]}{\Delta P_{eff}} \tag{40}$$

$$\lambda_p^2 = \frac{q_p[1 - (1 + C_{di})\lambda_1^2]}{\Delta P_{eff}} \tag{41}$$

The term $V_{p1}/V_{p\infty}$ can be expressed in terms of λ_1 and $q_e/\Delta P_{eff}$ with the aid of Equations 26, 28, and 30, which results in the expression

$$(V_{p\infty}/V_{p1})^2 = [1 - (1 + C_{di})\lambda_1^2][1 + q_e/\Delta P_{eff}] \tag{42}$$

Substituting Equations 40, 41, and 42 into Equation 39 provides the desired expression for the net thrust of an ejector.

$$F_{ej} = \frac{\rho a_\infty V_{p\infty}^2}{\sqrt{1 + \frac{q_e}{\Delta P_{eff}}}} \left\{ \left[\frac{[1+(\alpha-1)\lambda_1][1+(\overline{U_3'^2}/\bar{U}_3^2)]}{\alpha\delta^*\sqrt{1 - (1 + C_{di})\lambda_1^2}} - \sqrt{\frac{q_e}{\Delta P_{eff}}} \right] [1+(\alpha-1)\lambda_1] - \sqrt{\frac{q_p}{\Delta P_{eff}}} + \sqrt{\frac{q_e}{\Delta P_{eff}}} \right\} \tag{43}$$

where

a_∞ = nozzle exit area of the jet (at ambient pressure)

$V_{p\infty}$ = velocity of the reference jet exhaust after expansion from stagnation pressure to ambient pressure, with thrust efficiency η_N.

The net thrust of the reference jet (F_{ref}) is expressed as the net change of momentum of the pump mass flow after a lossless expansion from its stagnation pressure to ambient pressure.

$$F_{ref} = \rho a_\infty V_{p\infty}(V'_{p\infty} - U_p) \tag{44}$$

$$= \rho a_\infty V_{p\infty}^2 \frac{(1/\eta_N)\sqrt{1 + q_e/\Delta P_{eff}} - \sqrt{q_p/\Delta P_{eff}}}{\sqrt{1 + q_e/\Delta P_{eff}}} \tag{45}$$

and the thrust augmentation is then expressed as

$$\phi = \frac{F_{ej}}{F_{ref}} = \frac{\left[\frac{[1+(\alpha-1)\lambda_1][1+(\overline{U_3'^2}/\bar{U}_3^2)]}{\alpha\delta^*\sqrt{1-(1+C_{di})\lambda_1^2}} - \sqrt{\frac{q_e}{\Delta P_{eff}}}\right][1+(\alpha-1)\lambda_1] + \sqrt{\frac{q_e}{\Delta P_{eff}}} - \sqrt{\frac{q_p}{\Delta P_{eff}}}}{(1/\eta_N)\sqrt{1 + q_e/\Delta P_{eff}} - \sqrt{q_p/\Delta P_{eff}}} \tag{46}$$

for a solid diffuser ejector where all energized fluid is injected through primary nozzles. The value of λ_1 can be calculated using Equations 33 - 36. For an ideal ejector, the term $\delta^*/[1+(\overline{U_3'^2}/\bar{U}_3^2)]$ represents the geometric diffuser area ratio. Therefore, in the real fluid environment, the same term can be considered as a generalized diffuser area ratio, which includes the effects of flow separation and incomplete mixing, and can be estimated by the methods described in Section IV from experimental data.

2. Jet-Diffuser Ejector

a) Basic Theory

The analysis of a jet-diffuser ejector utilizes the identical formulation of the basic equations as for the solid diffuser, extended to include the diffuser jet region where appropriate.

The mathematical model of a jet-diffuser ejector, represented on Figure 1, illustrates the physical assumptions and the essential nomenclature.

The inlet drag is considered to be related to the dynamic pressure at the ejector's Station 1, similarly to the relationship (Equation 1) for a solid diffuser ejector

$$P_{oe} - P_{o1} = C_{di}(\rho/2)U_1^2 \tag{47}$$

which then translates into an effect on the Bernoulli constant as

$$p_1 - p_\infty = (\rho/2)[U_e^2 - U_1^2(1 + C_{di})] \tag{48}$$

or using the λ notation

$$p_1 - p_\infty = (\rho/2)V_{p1}^2[\lambda_e^2 - \lambda_1^2(1 + C_{di})] \tag{49}$$

The mass flow or continuity equation is also similar to that for the solid diffuser ejector, except for the fact that it is extended to include the core flow enclosed by the jet-diffuser, as follows.

$$X_1U_1 + a_1V_{p1} = X_2\bar{U}_2 = X_3\bar{U}_3 = X_4\bar{U}_4 \tag{50}$$

where,

X_3 is now considered to be the geometric cross-section of the solid diffuser surface, since flow separation is avoided.

X_4 is the effective area at the region where the flow has returned to ambient pressure.

Using the convenient notation

$$\alpha = X_2/a_1$$
$$\delta = X_3/X_2$$
$$\sigma = X_4/X_2 \qquad (51)$$
$$\lambda = \bar{U}/V_{pl}$$

the continuity equation takes the form

$$1 + (\alpha - 1)\lambda_1 = \alpha\lambda_2 = \alpha\delta\lambda_3 = \alpha\sigma\lambda_4 \qquad (52)$$

The flow through a jet-diffuser ejector returns to ambient pressure at Station 4 instead of Station 3 for a solid diffuser ejector. Since the mixing section (normally required for solid diffuser ejectors) is not required for jet-diffuser ejectors, and the diffuser jet emanates from a slot which is very close to the ejector's throat (Figure 5), the skin friction effect represented by C_F is replaced by the skin friction coefficient C_{fdj}, as will be described by Equation 57, for a jet-diffuser ejector. The law of conservation of mechanical energy between Stations 2 and 4 takes a form obtained by substitution of the subscipt 4 for subscript 3 in Equation 31, with C_F=0, thus,

$$\left[\lambda_4\left(1+\frac{\overline{U'^2_4}}{\bar{U}^2_4}\right)\right]^2 = [1-(1+C_{di})\lambda_1^2]\ (q_e/\Delta P_{eff}) + \left(\frac{1-\lambda_1^2}{\alpha^2}\right)\left[1 + \frac{2(\alpha - 1)}{1 + \lambda_1}\right] - C_{di}\lambda_1^2 \qquad (53)$$

and using Equation 52,

$$\frac{\sigma}{1 + (\overline{U'^2_4}/\bar{U}^2_4)} = \frac{1 + (\alpha - 1)\lambda_1}{\alpha\lambda_4[1 + (\overline{U'^2_4}/\bar{U}^2_4)]} \qquad (54)$$

The diffuser jet injection plane (Station J) is located within the solid surface (Figure 1), and encounters a skin friction dissipation of momentum between Stations J and 3. This loss must be considered in a real fluid determination of the influence of the stagnation pressure (P_{od}) on the fluid diffuser performance.

If an inviscid expansion of the diffuser jet mass flow occurs from its stagnation pressure to ambient pressure

$$(P_{od} - p_\infty) = (\rho/2)V_{d\infty}^2 \tag{55}$$

or

$$\dot{m}_d V_{d\infty} = 2(P_{od} - p_\infty)s_\infty \tag{56}$$

where

s_∞ = diffuser jet thickness which accomodates the mass flow $\dot{m}_d$, when exhausting to ambient pressure without loss

$\dot{m}_d$ = mass flow through diffuser jet

In the real, viscous case, if the skin friction force (f_{dj}) at the wetted surface between the diffuser jet and the wall is defined as

$$f_{dj} = (\rho/2)V_{d\infty}^2 C_{fdj}(2\ell_d) = \rho V_{d\infty}^2 s_\infty C_{fdj}(\ell_{dj}/X_2)(X_2/s_\infty) \tag{57}$$

where

ℓ_{dj} = arc length of solid surface between Stations J and 3

then

$$\dot{m}_d V_{d3} = \dot{m}_d V_{d\infty} - f_{dj} \tag{58}$$

$$= \rho V_{d\infty}^2 s_\infty [1 - C_{fdj}(\ell_{dj}/X_2)(X_2/s_\infty)] \tag{59}$$

To evaluate the "jet-flap" effect on the diffuser jet, assume that downstream of Station 3 neither the diffuser jet nor the core flow encounter any viscous dissipation. In order to evaluate the effect of the diffuser jet on the overall flowfield, the core flow is assumed uniform. In this situation the diffuser jet momentum ($\dot{m}_d V_{d3}$) issues at Station 3 as illustrated on Figure 2.

The momentum balance between Stations 3 and 4 provides the relationship

$$p_3 X_3 + 2\int_{X_3/2}^{X_4/2} p_- dy + \dot{m}_c \bar{U}_3 + \dot{m}_d V_{d3}\cos\beta = p_\infty X_4 + \dot{m}_d V_{d4} + \dot{m}_c \bar{U}_4 \tag{60}$$

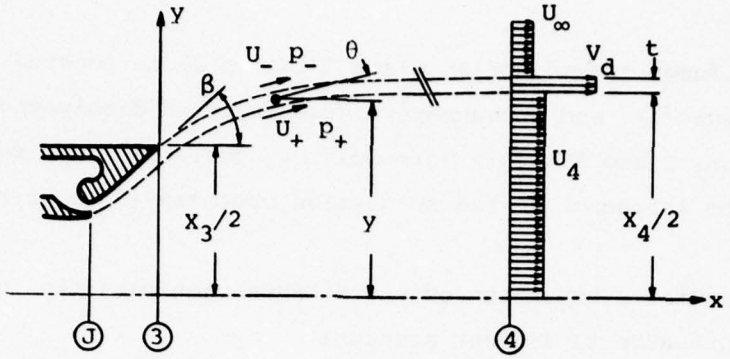

Figure 2. JET-DIFFUSER CONCEPT

In this analysis the accepted methods of thin airfoil and jet flap wing theory are used. Namely the jet sheet thickness compared to its radius of curvature is assumed small ($t/R \ll 1$). In addition the jet velocity is assumed large compared to the free stream or ejector exit velocities (U_∞ and U_4 respectively). Thus the jet sheet momentum can be shown to be constant and Equation 60 takes the form

$$(p_3 - p_\infty)X_3 + 2\int_{X_3/2}^{X_4/2} (p_- - p_\infty)dy + \dot{m}_c(\bar{U}_3 - \bar{U}_4) - \dot{m}_d V_d(1 - \cos\beta) = 0 \qquad (61)$$

since

$$\dot{m}_d V_d = \dot{m}_d V_{d3} = \dot{m}_d V_{d4} \text{ under the approximation of jet flap theory.} \qquad (62)$$

The non-homogeneous flow field comprising the diffuser jet and its immediate surroundings can be treated separately as follows.

The external and internal flows are equivalent to those which would exist if the jet were replaced by a vortex sheet. Thus a pressure differential would be created across the sheet due to the perturbation flowfield which in effect increases the velocity on one side and decreases the velocity by the same magnitude on the other side of the sheet. Then the local velocities differ from their undisturbed magnitudes by a small amount compared to the magnitude of the undisturbed velocities. Applying Bernoulli's Equation on each side of the jet sheet establishes the magnitude of the pressure difference as,

Internal (core) Flow,

$$p_\infty - p_+ = (\rho/2)(U_+^2 - \bar{U}_4^2) = (\rho/2)[(\bar{U}_4 + U')^2 - \bar{U}_4^2] \cong \rho\bar{U}_4 U' \qquad (63)$$

External Flow,

$$p_- - p_\infty = (\rho/2)(U_\infty^2 - U_-^2) = (\rho/2)[U_\infty^2 - (U_\infty - U')^2] \cong \rho U_\infty U' \tag{64}$$

and therefore

$$p_- - p_+ = p_{ext} - p_{int} = \rho U'(U_\infty + \bar{U}_4) \tag{65}$$

The pressure differential across the jet sheet can also be described by consideration of the momentum equation in the y-direction for the isolated jet sheet of thickness t. Thus from an arbitrary Station (x) to Station 4, the momentum law states that

$$\rho t V_d^2(\sin\theta - 0) = \int_x^\infty (p_- - p_+)dx \tag{66}$$

and noting that

$$\sin\theta = \frac{y'}{\sqrt{1 + y'^2}} \tag{67}$$

Equation 66 can be differentiated with respect to x. This yields the result

$$\rho t V_d^2 \frac{y''}{(1 + y'^2)^{3/2}} = -(p_- - p_+) \tag{68}$$

Therefore

$$p_- - p_+ = \frac{\rho t V_d^2}{R} = \dot{m}_d V_d/2R = \rho U'(U_\infty + \bar{U}_4) \tag{69}$$

since, for the jet sheet located at $y > 0$,

$$\frac{-y''}{(1 + y'^2)^{3/2}} = 1/R = \text{curvature} \tag{70}$$

and diffuser jet mass flow per unit length,

$$\dot{m}_d = (2t)\rho V_d$$

Thus, from Equation 69,

$$U' = \frac{\dot{m}_d V_d}{2\rho R(\bar{U}_4 + U_\infty)} \tag{71}$$

and therefore, using Equation 64,

$$p_- - p_\infty = \rho U_\infty U' = (\dot{m}_d V_d/2R)\,[U_\infty/(U_\infty + \bar{U}_4)] \tag{72}$$

Using Equation 72, the integral in Equation 61 can now be evaluated as follows.

$$\int_{X_3/2}^{X_4/2} (p_- - p_\infty)\,dy = [U_\infty/(U_\infty + \bar{U}_4)]\,(\dot{m}_d V_d/2) \int_{X_3/2}^{X_4/2} dy/R = [U_\infty/(U_\infty + \bar{U}_4)]\,(\dot{m}_d V_d/2)\,(1 - \cos\beta) \tag{73}$$

since

$$\int_{X_3/2}^{X_4/2} dy/R = \int_{\text{Sec.3}}^{\infty} \frac{-y'y''}{(1 + y'^2)^{3/2}}\,dx = \left[\frac{1}{\sqrt{1 + y'^2}}\right]_{y'=\tan\beta}^{y'=0} = 1 - \cos\beta$$

The remaining terms of Equation 61 can be expressed in the following convenient forms.

$$(p_3 - p_\infty)X_3 = (\rho/2)\,[\bar{U}_4^2 - \bar{U}_3^2]X_3 = (\rho/2)\bar{U}_4^2[1 - (X_4/X_3)^2]X_3 \tag{74}$$

and since

$$X_4/X_3 = \sigma/\delta \tag{75}$$

$$(p_3 - p_\infty)X_3 = (\rho/2)\lambda_4^2 V_{pl}^2 X_3[1 - (\sigma/\delta)^2] \tag{76}$$

The term $\dot{m}_c(\bar{U}_3 - \bar{U}_4)$ can be written as

$$\dot{m}_c(\bar{U}_3 - \bar{U}_4) = \rho X_4 \lambda_4^2 V_{pl}^2[\sigma/\delta - 1] \tag{77}$$

and inserting these terms into the basic form of Equation 61 results in the expression

$$\lambda_4^2(\sigma - \delta)^2 - 2(\delta/\alpha)(\dot{m}_d V_d/\dot{m}_p V_{pl})\,[1 - \lambda_\infty/(\lambda_\infty + \lambda_4)]\,(1 - \cos\beta) = 0 \tag{78}$$

b) Solution of Jet-Diffuser Ejector Problem

If both primary and diffuser jets are supplied by the same pump, the relationships among λ_∞, and $V_{d\infty}/V_{pl}$ and the geometric, operational and pump characteristics are,

$$\lambda_\infty^2 = \frac{q_\infty[1 - (1 + C_{di})\lambda_1^2]}{\Delta P_{eff}} \quad (79)$$

$$\dot{m}_d V_d/\dot{m}_p V_{pl} = (\dot{m}_d V_d/\dot{m}_d V_{d\infty})(\dot{m}_d V_{d\infty}/\dot{m}_p V_{pl})$$

and referring to Equations 59 and 62

$$\dot{m}_d V_d/\dot{m}_p V_{pl} = [1 - C_{fdj}(\ell_{dj}/X_2)(X_2/s_\infty)](\dot{m}_d/\dot{m}_p)(V_{d\infty}/V_{pl}) \quad (80)$$

also from Equations 24 and 42

$$V_{d\infty}/V_{pl} = V'_{p\infty}/V_{pl} = (1/\eta_N)\sqrt{[1 + (q_e/\Delta P_{eff})][1 - (1 + C_{di})\lambda_1^2]} \quad (81)$$

Define the last term of Equation 78 as H^2, then

$$H = \left\{\frac{2}{\eta_N}\left(\frac{\delta}{\alpha}\right)\left(\frac{\dot{m}_d}{\dot{m}_p}\right)(1-\cos\beta)\left[1-C_{fdj}\left(\frac{\ell_{dj}}{X_2}\right)\left(\frac{X_2}{s_\infty}\right)\right]\sqrt{[1-(1+C_{di})\lambda_1^2][1+(q_e/\Delta P_{eff})]}\left(1-\frac{\lambda_\infty}{\lambda_\infty+\lambda_4}\right)\right\}^{\frac{1}{2}} \quad (82)$$

Since λ_4 is inextricably associated with the non-uniformity parameter $\overline{U_4'^2}/\bar{U}_4^2$ in Equations 53 and 54, it is desirable to express H in terms of the same parameter.

Thus assuming that the non-uniformity parameter is small compared to 1.0,

$$\frac{\lambda_\infty}{\lambda_\infty + \lambda_4[1 + (\overline{U_4'^2}/\bar{U}_4^2)]} = \left[\frac{\lambda_\infty}{\lambda_\infty + \lambda_4}\right]\left[\frac{1}{1 + [\lambda_4/(\lambda_\infty + \lambda_4)](\overline{U_4'^2}/\bar{U}_4^2)}\right]$$

$$\simeq \left[\frac{\lambda_\infty}{\lambda_\infty + \lambda_4}\right]\left[1 - \frac{\lambda_4}{\lambda_\infty + \lambda_4}(\overline{U_4'^2}/\bar{U}_4^2)\right] \quad (83)$$

Therefore the correction term to be applied to H, to include the condition where $\lambda_\infty > 0$, can be expressed as

$$\frac{\lambda_\infty}{\lambda_\infty + \lambda_4} = \frac{\lambda_\infty}{\lambda_\infty + \lambda_4\left[1 + \left(\overline{U_4'^2}/\bar{U}_4^2\right)\right]} + \text{Order}\left[\overline{U_4'^2}/\bar{U}_4^2\right] \tag{84}$$

and the equation for H (Equation 82) can be approximated as

$$\tilde{H} = \left\{ \frac{2}{\eta_N}\left(\frac{\delta}{\alpha}\right)\left(\frac{\dot{m}_d}{\dot{m}_p}\right)(1-\cos\beta)\left[1-C_{fdj}\left(\frac{\ell_{dj}}{X_2}\right)\left(\frac{X_2}{s_\infty}\right)\right]\sqrt{\left(1-(1+C_{di})\lambda_1^2\right)\left(1+\frac{q_e}{\Delta P_{eff}}\right)} \right.$$

$$\left. \times \left[1 - \frac{\lambda_\infty}{\lambda_\infty + \lambda_4\left[1+\left(\overline{U_4'^2}/\bar{U}_4^2\right)\right]}\right] \right\}^{\frac{1}{2}} \tag{85}$$

and since $\sigma \geq \delta$, Equation 78 becomes

$$\sigma = \delta + H/\lambda_4$$

and expressing λ_4 in terms of λ_1 using Equation 52, results in the expression

$$\sigma = \frac{\delta}{1 - \dfrac{\alpha H}{1 + (\alpha - 1)\lambda_1}} \qquad \text{(ideal)} \tag{86}$$

Equation 86 describes the ideal relationship among the effective diffuser area ratio (σ) of a jet-diffuser ejector, its geometric diffuser area ratio (δ), its diffuser jet characteristic (H), and λ_1. In the real ejector, discrepancies exist, due to non-uniformity of jet thickness, non-uniform diffuser jet exit angle (β), such as flat end jet-diffuser ejectors where $\beta_{end} = 0$, which cannot accept pressure gradient across the jet sheet, etc. Therefore, it is necessary to introduce an empirical constant to modify Equation 86.

$$\sigma = \eta'_{dj} \left[\frac{\delta}{1 - \frac{\alpha H}{1 + (\alpha - 1)\lambda_1}} \right] \tag{87}$$

The empirical constant η'_{dj} can be combined with the nonuniformity paramter $\overline{U'^2_4}/\bar{U}^2_4$ in a more useful form as

$$\eta_{dj} = \frac{\eta'_{dj}}{1 + (\overline{U'^2_4}/\bar{U}^2_4)} \tag{88}$$

then

$$\frac{\sigma}{1 + (\overline{U'^2_4}/\bar{U}^2_4)} = \eta_{dj} \left[\frac{\delta}{1 - \frac{\alpha H}{1 + (\alpha - 1)\lambda_1}} \right] \tag{89}$$

It is worth noting that for a perfect jet-diffuser ejector, the mixing process can be carried out to its ultimate conclusion within the jet-diffuser boundary, or $\overline{U'^2_4}/\bar{U}^2_4 = 0$. In this case, Equations 86 and 89 are identical if $\eta_{dj} = 1$. Therefore, the factor η_{dj} represents the 'efficiency' of the jet-diffuser design, which includes the consideration of incomplete mixing.

Equations 53, 54, 85 and 89 describe a complete solution of the jet-diffuser ejector equations with four empirical constants (η_N, C_{di}, C_{fdj} and η_{dj}) and four dependent variables, $\lambda_4[1 + (\overline{U'^2_4}/\bar{U}^2_4]$, $\sigma/ [1 + (\overline{U'^2_4}/\bar{U}^2_4)]$, λ_1 and H.

c) Performance of Jet-Diffuser Ejector

1) Thrust Augmentation

With the solution for $\lambda_4[1 + (\overline{U_4'^2}/\bar{U}_4^2)]$, the thrust augmentation (ϕ) can be evaluated for the general case of the ejector in motion with boundary layer intake at the ejector and at the pump inlet as follows:

The net thrust (gross thrust minus ram drag) of the ejector (F_{ej}), is the sum of net thrust of the core flow, plus that of the diffuser jet, thus,

$$F_{ej} = \rho a_\infty V_{p\infty}^2 (V_{pl}/V_{p\infty}) \left\{ \alpha\sigma\lambda_4 \left[\lambda_4 [1 + (\overline{U_4'^2}/\bar{U}_4^2)] - \lambda_e \right] + \lambda_e - \lambda_p + (\dot{m}_d/\dot{m}_p)(\lambda_d - \lambda_p) \right\} \tag{90}$$

where

$$\lambda_d = V_d/V_{pl} = (V_{d\infty}/V_{pl}) \left[1 - C_{fd} (\ell_{dj}/X_2)(X_2/s_\infty) \right] \tag{91}$$

and $V_{d\infty}/V_{pl}$ is given by Equation 81.

The thrust of a reference jet(F_{ref}) which has a mass flow equal to the sum of the mass flows of the ejector's primary and diffuser jets and which has the same plenum pressure ($P_{op} = P_{od}$) as those of the primary and diffuser jet is

$$F_{ref} = \rho a_\infty V_{p\infty} (V'_{p\infty} - U_p)[1 + (\dot{m}_d/\dot{m}_p)]$$

$$= \rho a_\infty V_{p\infty}^2 [1 + (\dot{m}_d/\dot{m}_p)] \frac{(1/\eta_N)\sqrt{1 + q_e/\Delta P_{eff}} - \sqrt{q_p/\Delta P_{eff}}}{\sqrt{1 + q_e/\Delta P_{eff}}} \tag{92}$$

If we define thrust augmentation as

$$\phi = F_{ej}/F_{ref} \tag{93}$$

the general expression can be written as

$$\phi = \left\{ \left[1 + (\alpha - 1)\lambda_1 \right] \left[\frac{\lambda_4 \left(1 + \frac{\overline{U_4'^2}}{\overline{U}_4^2} \right)}{\sqrt{1 - (1 + C_{di})\lambda_1^2}} - \sqrt{\frac{q_e}{\Delta P_{eff}}} \right] + \sqrt{\frac{q_e}{\Delta P_{eff}}} - \sqrt{\frac{q_p}{\Delta P_{eff}}} \right.$$

$$\left. + \left(\frac{\dot{m}_d}{\dot{m}_p} \right) \left[\frac{1}{\eta_N} \sqrt{1 + \frac{q_e}{\Delta P_{eff}}} \left[1 - C_{fdj} \left(\frac{\ell_{dj}}{X_2} \right) \left(\frac{X_2}{s_\infty} \right) \right] - \sqrt{\frac{q_p}{\Delta P_{eff}}} \right] \right\}$$

$$\div \left\{ \left[1 + \frac{\dot{m}_d}{\dot{m}_p} \right] \left[\frac{1}{\eta_N} \sqrt{1 + \frac{q_e}{\Delta P_{eff}}} - \sqrt{\frac{q_p}{\Delta P_{eff}}} \right] \right\} \tag{94}$$

2) Propulsive Efficiency

The propulsive efficiency (η) of a jet or an ejector is defined conventionally as the ratio of thrust power to jet power.

$$\eta_{ej} = \frac{\text{Thrust x Velocity}}{\text{Jet Power}} = \frac{[\dot{m}_p (V'_{p\infty} - U_p) + \dot{m}_d (V_{d\infty} - U_p)] U_\infty \phi}{1/2 [\dot{m}_p (V'^2_{p\infty} - U_p^2) + \dot{m}_d (V^2_{d\infty} - U_p^2)]} \tag{95}$$

when $V'_{p\infty} = V_{d\infty}$, this reduces to the form

$$\eta_{ej} = \frac{2 (U_\infty / V'_{p\infty}) \phi}{1 + (U_p / V'_{p\infty})} = \phi \eta_{ref} \tag{96}$$

where

$$(U_\infty / V'_{p\infty})^2 = [q_\infty / (\Delta P + q_p)] \tag{97}$$

Using this relationship, the propulsive efficiency can be written in the form

$$\eta_{ej} = \frac{2\phi\sqrt{q_\infty/\Delta P}}{\sqrt{1 + (q_p/\Delta P)} + \sqrt{q_p/\Delta P}} \tag{98}$$

3) Relative Power (R_p)

Relative power is defined herein as the ratio of the jet power required by an ejector to that required by a free jet having the same net thrust and energized mass flow as the ejector.

A free jet of area a_o develops a net thrust F_o having a magnitude

$$F_o = \rho a_o V_{j,o}(V_{j,o} - U_p) \tag{99}$$

where $V_{j,o}$ is the jet velocity relative to the vehicle.

The power required to drive this free jet ($P_{j,o}$) is

$$P_{j,o} = (1/2)(\rho a_o V_{j,o})(V_{jo}^2 - U_p^2) \tag{100}$$

where $\rho a_o V_{j,o}$ is the mass flow of the free jet.

An ejector has a net thrust F_{ej} whose magnitude in terms of the injected fluid characteristics and its thrust augmentation is

$$F_{ej} = [\dot{m}_p(V'_{p\infty} - U_p) + \dot{m}_d(V_{d\infty} - U_p)]\phi \tag{101}$$

where

$V'_{p\infty}$ = velocity of primary jet after lossless expansion to ambient pressure

$V_{d\infty}$ = velocity of diffuser jet after lossless expansion to ambient pressure

If $V'_{p\infty} = V_{d\infty} = V_{j\infty}$

$$F_{ej} = \dot{m}_p\{(V_{j\infty} - U_p)[1 + (\dot{m}_d/\dot{m}_p)]\}\phi \tag{102}$$

the power required by this ejector is $P_{j,ej}$

$$P_{j,ej} = 1/2\ \dot{m}_p(V'^2_{p\infty} - U_p^2) + 1/2\ \dot{m}_d(V_{d\infty}^2 - U_p^2)$$

or

$$P_{j,ej} = 1/2\ \dot{m}_p\{(V_{j\infty}^2 - U_p^2)[1 + (\dot{m}_d/\dot{m}_p)]\} \tag{103}$$

where $\dot{m}_p[1 + (\dot{m}_d/\dot{m}_p)]$ is the total energized mass flow.

Assume that the two devices have the same thrust and energized mass flow. Then the power ratio $(P_{j,ej}/P_{j,o}) = R_p$ is

$$R_p = \frac{(V_{j\infty} + U_p)(V_{j\infty} - U_p)}{(V_{j,o} + U_p)(V_{j,o} - U_p)} \tag{104}$$

and the equality of their thrusts and mass flow rate provides the relationship

$$(V_{j\infty} - U_p)\phi = V_{j,o} - U_p \tag{105}$$

or

$$\phi(V_{j\infty} + U_p) = (V_{j,o} + U_p) + 2U_p(\phi - 1) \tag{106}$$

thus

$$\frac{V_{j,o} + U_p}{V_{j\infty} + U_p} = \phi - \frac{2U_p}{V_{j\infty} + U_p}(\phi - 1) \tag{107}$$

and

$$\frac{V_{j,o} - U_p}{V_{j\infty} - U_p} = \phi \tag{108}$$

Eliminating $V_{j,o}$ from Equation 104, using Equations 107 and 108

$$1/R_p = \phi^2 - \frac{2\phi U_p}{V_{j\infty} + U_p}(\phi - 1)$$

$$= \phi^2 - \phi \frac{2U_p/V_{j\infty}}{1 + U_p/V_{j\infty}}(\phi - 1) \tag{109}$$

and since

$$\eta_{ej} = \frac{2U_\infty/V_{j\infty}}{1 + U_p/V_{j\infty}}\phi \tag{110}$$

$$1/R_p = \phi^2 - \eta_{ej}(\phi - 1)(U_p/U_\infty) \tag{111}$$

IV METHODS FOR EVALUATION OF EJECTOR LOSS COEFFICIENTS FROM EXPERIMENTAL DATA

To determine the performance of an ejector in a realistic manner, from purely analytical considerations, it is essential that the loss factors be accurately known.

These loss factors can be evaluated in a variety of ways; some discussion of these methods exists in the literature. However, the precise method for evaluation of ejector losses, particularly those factors related to incomplete mixing or flow non-uniformity have never been treated in a consistent manner for inclusion in the flow and performance equations.

This section is therefore devoted to descriptions of suggested methods, consistent with the previous analysis, for determination of the factors influencing ejector performance, which do not naturally enter the conventional analyses of ideal ejector flow.

1. Inlet Drag

All ejectors encounter a loss during the process of capture of ambient or induced flow, due to the obstruction of primary jet ducts and skin friction and inlet separation on the inlet lips.

To evaluate this loss in terms of the theoretical model depicted on Figure 1, and to realistically account for the flow non-uniformity resulting from inlet surface and streamline curvature, the throat or survey station is assumed to exist at Station x, as illustrated on Figure 3 below.

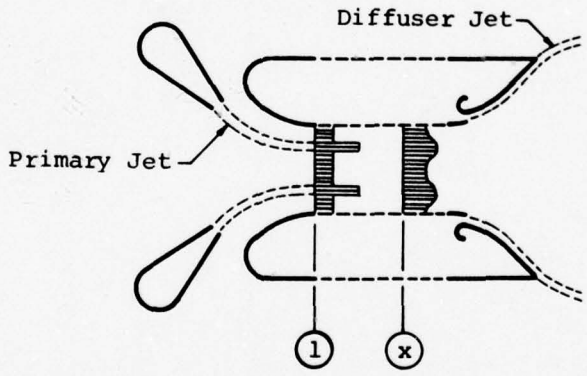

FIGURE 3. ANALYTICAL MODEL ILLUSTRATING ASSUMED LOCATION OF STATION x

At Station x, the flow is non-uniform (mixing is in progress) and all inlet losses have already occurred.

In this case, the momentum equation between Stations 1 and x, where the area remains constant, can be written as

$$\alpha(\bar{p}_x - p_1) = \rho V_{p1}^2 \{1 + (\alpha - 1)\lambda_1^2\} - \alpha\rho\overline{U_x^2} \tag{112}$$

where

$$\bar{p}_x = (1/A_2) \int_{A_2} p_x dA$$

$$\bar{U}_x = (1/A_2) \int_{A_2} U_x dA \tag{113}$$

$$\overline{U_x^2} = (1/A_2) \int_{A_2} U_x^2 dA$$

Since in a real ejector, Station 1 does not usually exist (flow at the throat is partially mixed and the pressure is not uniform), the quantities in Equation 112 referred to Station 1 (λ_1, α, p_1, V_{p1}) must be expressed in terms of other "measurable" quantities, thus,

$$r = \dot{m}_i/\dot{m}_p = (\dot{m}_c/\dot{m}_p) - 1 = (1/\dot{m}_p) \int_{A_2} \rho U_x dA - 1 = (\rho \bar{U}_x A_2/\dot{m}_p) - 1 \tag{114}$$

also, since

$$r = (\alpha - 1)\lambda_1$$

$$\alpha = (r + \lambda_1)/\lambda_1 \tag{115}$$

but from Equation 42,

$$(V_{p\infty}/V_{p1})^2 = (\alpha_\infty/\alpha)^2 = [1 - (1 + C_{di})\lambda_1^2][1 + (q_e/\Delta P_{eff})] \tag{116}$$

where

$$\alpha_\infty = A_2/a_\infty = \rho V_{p\infty} A_2/\dot{m}_p = \frac{A_2\sqrt{2\rho(\Delta P_{eff} + q_e)}}{\dot{m}_p} \tag{117}$$

Therefore

$$(V_{p\infty}/V_{pl})^2 = [1 - (1 + C_{di})\lambda_1^2][1 + q_e/\Delta P_{eff}] = (\alpha_\infty/\alpha)^2 = \alpha_\infty^2[\lambda_1/(r + \lambda_1)]^2 \quad (118)$$

from Equation 3,

$$p_1 = p_\infty + q_e - (\rho/2)V_{pl}^2(1 + C_{di})\lambda_1^2 \quad (119)$$

Performing the indicated algebraic substitutions, Equation 112 takes the form

$$\zeta\alpha_\infty^2[\lambda_1/(r + \lambda_1)]^2 + 2(1 + r\lambda_1)[\lambda_1/(r + \lambda_1)] - 1 = 0 \quad (120)$$

where

$$\zeta = \frac{p_\infty + q_e - \bar{p}_x - \rho\overline{u_x^2}}{(\rho/2)V_{p\infty}^2} + \frac{1}{1 + q_e/\Delta P_{eff}} = 1 - \frac{\overline{(p_\infty - p_x)} + 2\overline{(p_{tx} - p_\infty)}}{\Delta P_{eff} + q_e} \quad (121)$$

Note that from Equation 30, $\Delta P_{eff} + q_e = \eta_N^2(\Delta P + q_p)$
where p_{tx} is the total pressure distribution at the survey section.

Equation 120 is a cubic equation involving λ_1, which can be expressed in a more conventional form as

$$\lambda_1^3 + \left[\frac{2r^2 + \alpha_\infty^2\zeta + 1}{2r}\right]\lambda_1^2 - r/2 = 0 \quad (122)$$

where all quantities other than λ_1 are determinable from conventional ejector experiments and a survey of stagnation and static pressure at Station x.

Solution of Equation 122 provides the quantity λ_1 for any given experimental set-up, and having this value and the entrainment ratio, r, (Equation 114) and α_∞ (Equation 117), the inlet drag coefficient (C_{di}) can be evaluated since, from Equation 118,

$$C_{di} = \frac{\left[1 - \frac{\alpha_\infty^2}{1 + q_e/\Delta P_{eff}}\left(\frac{\lambda_1}{r + \lambda_1}\right)^2\right]}{\lambda_1^2} - 1 \quad (123)$$

This method for the determination of C_{di} requires a survey at the ejector's throat for evaluation of ζ and of λ_1. Such data does not exist in an incompressible fluid and in its absence, data from experiments in air must be utilized.

It should be noted however, that experiments in air require an additional survey at Station x measuring the temperature distribution for accurate evaluation of the compressibility effect.

This type of data is not presently available and values of C_{di} can only be obtained by other less reliable experimental techniques.

Quinn, (Reference 4) for example, has reported C_{di} for the ejectors developed at the Aerospace Research Laboratory in AIAA Paper No. 72-1174. His estimate of $C_{di} = 0.025$ will be used for correlation of the ejector data with a hypermixing primary nozzle.

Experimental determination of the inlet drag coefficient for the STAMP AJDE was performed at FDRC, using an assumed uniform total temperature equal to the mass flow averaged total temperature of primary and induced flows and compressible flow equations, parallel to those presented here, but not described since they are beyond the scope of this document.

The results of this experimental analysis yielded inlet drag coefficients (C_{di}), ranging from 0.013 to 0.016, for the jet-diffuser ejector, depending upon primary nozzle design and attitude. Since the AJDE has throat dimensions of 10.16 cm x 38.1 cm, the two-dimensional value of C_{di} is about 0.010 to 0.013.

2. Skin Friction, Diffuser Performance, and Incomplete Mixing

The skin friction phenomenon differs considerably depending upon the type of ejector being considered. Therefore, the method for evaluation of this quantity will be discussed separately for the solid diffuser and the jet-diffuser ejector.

a) Solid Diffuser

Since the skin friction in a solid diffuser ejector occurs in its mixing section and in its diffuser, the integrated effect is combined into a single coefficient C_F, described by Equation 21, in terms of its component parts.

The evaluation of C_F from experiments on solid diffuser ejectors can be made in terms of λ_1 ($= U_1/V_{p1}$), ϕ, η_N, and C_{di} for any given set of operational, injected fluid and ejector geometric conditions.

If λ_1, ϕ, η_N, and C_{di} are known (either from experiment or analysis), the value of C_F can be determined as follows, for a solid diffuser ejector.

Rearrangement of Equation 46 results in the expression

$$\frac{\frac{\delta^*}{}}{1+(\overline{U_3'^2}/\bar{U}_3^2)} = \frac{[1+(\alpha-1)\lambda_1]^2}{\alpha\sqrt{1-(1+C_{di})\lambda_1^2}\left\{\phi\left[\frac{1}{\eta_N}\sqrt{1+q_e/\Delta P_{eff}}-\sqrt{q_p/\Delta P_{eff}}\right]+\sqrt{q_p/\Delta P_{eff}}+(\alpha-1)\lambda_1\sqrt{q_e/\Delta P_{eff}}\right\}} \tag{124}$$

Substituting Equation 5 into Equation 31, and solving for C_F,

$$C_F = \left[\frac{\alpha}{1+(\alpha-1)\lambda_1}\right]^2\left\{[(1-\lambda_1^2)/\alpha^2]\left[1+\frac{2(\alpha-1)}{1+\lambda_1}\right]-C_{di}\lambda_1^2+[1-(1+C_{di})\lambda_1^2]q_e/\Delta P_{eff}\right\}$$

$$-\left[\frac{1+(\overline{U_3'^2}/\bar{U}_3^2)}{\delta^*}\right]^2 \tag{125}$$

Elimination of the quantity $[1 + (\overline{U_3'^2}/\bar{U}_3^2)]/\delta^*$ from Equations 124 and 125 leads to the relationship among ϕ, C_F, and λ_1, for any known values of α, C_{di}, η_N, $q_p/\Delta P_{eff}$, and $q_e/\Delta P_{eff}$. Therefore, C_F can be determined if experimental values of ϕ, λ_1, α, η_N, C_{di}, $q_p/\Delta P_{eff}$, and $q_e/\Delta P_{eff}$ are known.

Unfortunately, the value of λ_1 is seldom known accurately and the above method may produce results which are easily shown to be inconsistent with physical realities.

For example, in the above referenced report by Quinn of Aerospace Research Laboratories, the thrust augmentation of five different solid diffuser ejectors tested under stationary conditions is presented along with information about the systematic variation of mixing section and diffuser lengths. Values of λ_1 determined by pressure taps in the throat are also presented for Configuration D.

The ARL ejector has a rectangular throat of 10" wide by 60" long, with an inlet area ratio $\alpha = 25.3$, and the inlet drag coefficient $C_{di} = 0.025$. Configurations A, B, C, D, and F have straight diffuser walls with different lengths of constant area mixing ducts. Their total lengths after primary fluid injection are $\ell_T/X_2 = 4.525$; 2.825; 2.8; 5; and 5 respectively. Experimental values of ϕ vs. δ are available for all five configurations. Values of λ_1 for Configuration D are also given.

According to the author, the internal flow of the hypermixing nozzles experiences relatively high loss, so that the thrust efficiency of the nozzle is only $\eta_N = 0.96$.

The coefficient of skin friction, C_f, is estimated by the application of Equations 124, 21, and 125 to values of ϕ, and λ_1 reported for Configuration D. Except for $\delta = 1$ (which has an exceptionally low C_f), the value of C_f, determined in this manner, is between 0.008 and 0.011. After correction for the aspect ratio effect to account for the skin friction on the end wall by dividing C_f by (1 + 1/6), the coefficient of skin friction (C_f) based on the wetted surface area is between 0.007 and 0.009.

This high value of the coefficient of skin friction is believed to result from the questionable experimental technique of using a single static pressure measurement to determine the parameter λ_1. As mentioned before, extensive flow surveys in the throat are required to obtain a reliable value of λ_1, due to the complexity of the ejector flow.

However, there is a specific maximum value of C_f which can satisfy all the data of Configurations A, B, C, D, and F to provide the physical restriction that

$$(\delta/\delta^*)\left[1 + (\overline{u_3'^2}/\bar{u}_3^2)\right] \geq 1$$

a condition which must be satisfied since

$$\delta^* \leq \delta \qquad \text{and} \qquad (\overline{u_3'^2}/\bar{u}_3^2) \geq 0$$

This value of C_f is about 0.0057. After correcting for the aspect ratio effect by dividing by (7/6), as discussed earlier, the coefficient of skin friction based on the wetted surface area becomes 0.0049, which is the typical value for a flat plate turbulent boundary layer over a wide range of Reynolds Numbers near 10^6.

If surveys of the ejector's throat section are not available, the value of λ_1 cannot be determined as described by Equations 121 and 122. However, if C_F is evaluated by conventional boundary layer theory in terms of the Reynolds Number, and if C_{di} and the geometric, operational, and injected fluid characteristis are known, the value of λ_1 can be determined by the following method.

Eliminate $\delta^*/[1 + (\overline{U_3'^2}/\overline{U}_3^2)]$ from Equations 124 and 125. This procedure results in a quartic equation of the form

$$b_0 + b_1\lambda_1 + b_2\lambda_1^2 + b_3\lambda_1^3 + b_4\lambda_1^4 = 0 \tag{126}$$

where

$$b_0 = C_F + \alpha^2(\phi')^2 - (2\alpha - 1) - \alpha^2(q_e/\Delta P_{eff})$$

$$b_1 = 2(\alpha - 1)\left\{2C_F - 2(\alpha - 1) + \alpha^2\left[\phi' - \sqrt{q_e/\Delta P_{eff}}\right]\sqrt{q_e/\Delta P_{eff}}\right\}$$

$$b_2 = (\alpha - 1)^2[6C_F - 2\alpha + 5] - \alpha^2[(\phi')^2 - q_e/\Delta P_{eff}](1 + C_{di}) + \alpha^2 C_{di} + 1$$

$$b_3 = 2(\alpha-1)^3[2C_F+1]+2\left\{1+ \alpha^2C_{di} - \alpha^2(1+C_{di})\left[\phi' -\sqrt{q_e/\Delta P_{eff}}\right]\sqrt{q_e/\Delta P_{eff}}\right\}(\alpha-1)$$

$$b_4 = C_F(\alpha - 1)^4 + (1 + \alpha^2 C_{di})(\alpha - 1)^2$$

where

$$\phi' = \phi\left[(1/\eta_N)\sqrt{1 + q_e/\Delta P_{eff}} - \sqrt{q_p/\Delta P_{eff}}\right] + \sqrt{q_p/\Delta P_{eff}}$$

A solution of this equation provides the value of λ_1, in terms of quantities which are known or easily measured experimentally. Hence, instead of relying upon the measurement of λ_1, λ_1 can be calculated by the assumed value of $C_f = 0.0057$ and the measured ϕ from Equations 126 and 21. After obtaining the value of λ_1, the quantity $[1 + (\overline{U_3'^2}/\overline{U}_3^2)]/\delta^*$ can be calculated by using Equation 124. Figure 4 summarizes this effort for all five configurations.

The average value of $(\delta/\delta^*)[1 + (\overline{U_3'^2}/\overline{U}_3^2)]$ for Configuration F is about 1.05. This value appears to be adequate for the low δ range of all other configurations under consideration.

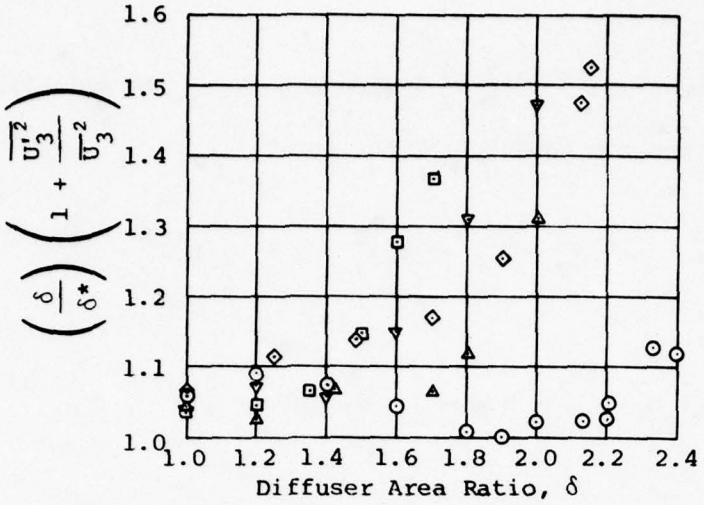

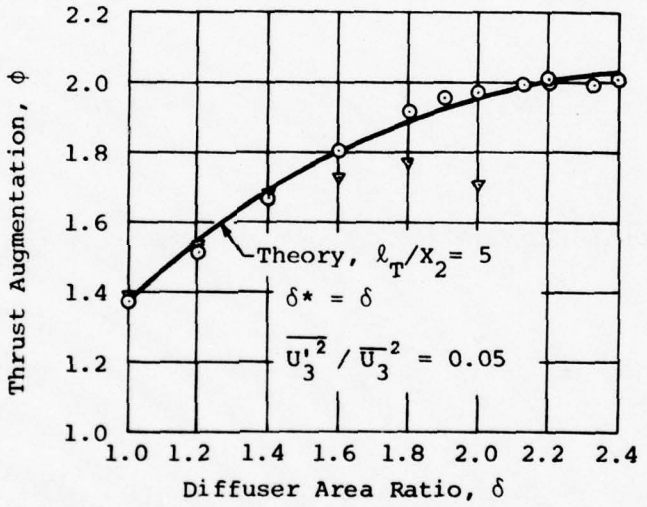

ARL Ejector (AIAA Paper 72-1174)

α = 25.3; η_N = 0.96; C_{di} = 0.025

C_f = 0.0057 (assumed)

Configuration	Symbol	ℓ_T/X_2
A	△	4.525
B	⊡	2.825
C	◇	2.8
D	▼	5
F	⊙	5

Figure 4. CORRELATION OF THEORY WITH ARL EJECTORS

One simple method for evaluation of the non-uniformity parameter $\overline{u_3'^2}/\bar{u}_3^2$ consists of the use of an ejector test where no separation exists in the diffuser. Then $\delta^* = \delta$ and the value of the non-uniformity parameter $\overline{u_3'^2}/\bar{u}_3^2$ can be determined from the identity

$$\overline{u_3'^2}/\bar{u}_3^2 = \left[\frac{1 + (\overline{u_3'^2}/\bar{u}_3^2)}{\delta^*}\right]\delta - 1 \qquad (127)$$

Therefore, for non-separating ARL ejectors, ($\delta = \delta^*$), the non-uniformity parameter is about 0.05, or,

$$\overline{u_3'^2}/\bar{u}_3^2 = 0.05$$

Both Configurations D and F have a $\ell_T/X_2 = 5$, and Configuration F is the best performing ARL Ejector. By assuming $\delta^* = \delta$, and using the parameters derived from the above discussion, ϕ can be calculated by using Equations 46, 33 to 36, and 5. The result is shown on Figure 4. As can be seen, Configuration F follows closely to the theory, which means that the assumption $\delta^* = \delta$ holds, and the flow is probably free from separation for the range tested. However, the assumption of $\delta^* = \delta$ breaks down for Configuration D near $\delta = 1.4$, which indicates that Configuration D experienced flow separation near $\delta = 1.4$. The lower performance of Configuration D is apparently due to the failure of its diffuser.

b) Jet-Diffuser Ejector

1) Diffuser Performance

Equation 53 for the jet-diffuser ejector can be rewritten by using Equation 52 to obtain

$$\frac{\sigma}{1 + (\overline{U_4'^2}/\bar{U}_4^2)} = \frac{1+(\alpha-1)\lambda_1}{\alpha}\left\{\frac{1-\lambda_1^2}{\alpha^2}\left[1+\frac{2(\alpha-1)}{1+\lambda_1}\right] - C_{di}\lambda_1^2 + [1-(1+C_{di})\lambda_1^2](q_e/\Delta P_{eff})\right\}^{\frac{1}{2}} \tag{128}$$

Also, rewrite Equation 94 by using Equation 52

$$\frac{\sigma}{1 + (\overline{U_4'^2}/\bar{U}_4^2)}$$

$$= \frac{[1 + (\alpha-1)\lambda_1]^2}{\alpha\sqrt{1 - (1+C_{di})\lambda_1^2}} \div \left\{\phi\left[1 + \frac{\dot{m}_d}{\dot{m}_p}\right]\left[\frac{1}{\eta_N}\sqrt{1+\frac{q_e}{\Delta P_{eff}}} - \sqrt{\frac{q_p}{\Delta P_{eff}}}\right] + \sqrt{\frac{q_p}{\Delta P_{eff}}}\right.$$

$$\left. + (\alpha-1)\lambda_1\sqrt{\frac{q_e}{\Delta P_{eff}}} - \frac{\dot{m}_d}{\dot{m}_p}\left[\frac{1}{\eta_N}\sqrt{1+\frac{q_e}{\Delta P_{eff}}}\left[1 - C_{fdj}\left(\frac{\ell_{dj}}{X_2}\right)\left(\frac{X_2}{s_\infty}\right)\right] - \sqrt{\frac{q_e}{\Delta P_{eff}}}\right]\right\} \tag{129}$$

since α and α_∞ are related by

$$\alpha = \frac{\alpha_\infty}{\sqrt{1 - (1 + C_{di})\lambda_1^2}\sqrt{1 + (q_e/\Delta P_{eff})}} \tag{130}$$

The system of three equations, 128, 129, and 130, has four unknowns; α, λ_1, C_{fdj}, and $\sigma/[1 + (\overline{u_4'^2}/\bar{u}_4^2)]$. Thus, if λ_1 can be measured experimentally, C_{fdj} can be calculated. However, due to the complexity involved in measuring λ_1 as discussed previously C_{fdj} will be estimated, then calculate λ_1.

From Equation 85,

$$H = \left\{ \frac{2}{\eta_N}\left(\frac{\delta}{\alpha}\right)\left(\frac{\dot{m}_d}{\dot{m}_p}\right)(1 - \cos\beta)\left[1 - C_{fdj}\left(\frac{\ell_{dj}}{X_2}\right)\left(\frac{X_2}{s_\infty}\right)\right]\sqrt{\left[1 - (1 + C_{di})\lambda_1^2\right]\left(1 + \frac{q_e}{\Delta P_{eff}}\right)} \right.$$

$$\left. \times \left[1 - \frac{\lambda_\infty}{\lambda_\infty + \lambda_4[1 + (\overline{u_4'^2}/\bar{u}_4^2)]}\right] \right\}^{1/2} \qquad (131)$$

where

$$\lambda_\infty = \sqrt{\left[1 - (1 + C_{di})\lambda_1^2\right]\frac{q_\infty}{\Delta P_{eff}}} \qquad (132)$$

and

$$\lambda_4[1 + (\overline{u_4'^2}/\bar{u}_4^2)] = \frac{1 + (\alpha - 1)\lambda_1}{\alpha}\left[\frac{1 + (\overline{u_4'^2}/\bar{u}_4^2)}{\sigma}\right] \qquad (133)$$

Therefore the solution of the system of Equations 128, 129, and 130, with estimated C_{fdj}, provides the values of α, λ_1 and $\{\sigma/[1 + (\overline{u_4'^2}/\bar{u}_4^2)]\}$, and the value of H (from Equations 131 to 133). By knowing these values, η_{dj} can be calculated from Equation 89,

$$\eta_{dj} = \left[\frac{\sigma}{1 + (\overline{u_4'^2}/\bar{u}_4^2)}\right]\left\{\frac{1 - \frac{\alpha H}{1 + (\alpha - 1)\lambda_1}}{\delta}\right\} \qquad (134)$$

2) Skin Friction Coefficient, C_{fdj}

The value of C_{fdj}, the skin friction coefficient, can be established from the Blasius Law for Reynolds Numbers less than 5×10^5 (laminar boundary layer), where the Reynolds Number is based upon the length of the wetted surface, and by the Prandtl-Schlichting Law for Reynolds Numbers greater than or equal to 5×10^5 (transition and turbulent boundary layers).

Thus,

$$Re_{\ell} = \rho V_{d\infty} \ell_{dj} / \mu \tag{135}$$

where

$$V_{d\infty} = \sqrt{(2/\rho)(\Delta P)[1 + (q_p/\Delta P)]} \tag{136}$$

and therefore

$$Re_{\ell} = (1/\mu)(\ell_{dj}/X_2) X_2 \sqrt{2\rho(\Delta P)[1 + (q_p/\Delta P)]} \tag{137}$$

and in water (20°C)

$$\mu = 1 \times 10^{-3} \text{ kg/m-sec} \tag{138}$$

and therefore

$$Re_{\ell} = 45{,}300(\ell_{dj}/X_2) X_2 \sqrt{(\Delta P)[1 + (q_p/\Delta P)]} \tag{139}$$

where X_2 in meters, ΔP in Newtons/m^2 or Pascals.
For example, one of the jet-diffuser ejectors developed by FDRC has a two-dimensional geometry such that

$$\ell_{dj}/X_2 = 0 \qquad \delta \leq 1.0304 \tag{140}$$

$$\ell_{dj}/X_2 = 1.0999\delta - 1.1333 \qquad 1.0304 < \delta < 1.5855 \tag{141}$$

$$\ell_{dj}/X_2 = 0.7071\delta - 0.5105 \qquad \delta \geq 1.5855 \tag{142}$$

$$X_2 = 10.16 \text{ cm}$$

Using the skin friction laws refered to above,

$$C_{fdj} = 1.328/\sqrt{Re_\ell} \qquad Re_\ell < 5 \times 10^5 \tag{143}$$

$$C_{fdj} = 0.455/(\log Re_\ell)^{2.58} - 1614/Re_\ell \qquad Re_\ell \geq 5 \times 10^5 \tag{144}$$

determines the value of C_{fdj} for any given operating conditions.

3) Correlation with Stationary Experiments

There are two types of jet-diffuser ejectors developed by the Flight Dynamics Research Corporation:

1) Quasi-two-dimensional or STAMP AJDE (Reference 1)

   This type of AJDE requires flat end plates protruding beyond the exit of the diffuser to ensure proper function of the jet-diffuser. The diffuser jet assigned to the ejector ends serves the function of boundary layer control only, and does not contribute to the jet diffusion ($\beta = 0$).

2) Three-dimensional AJDE (Reference 5)

   This ejector eliminates the requirement for flat end plates while it improves its performance by using potential flow theory as a design tool, for the shape of the ends of the rectangular ejector.

Since only very limited data is available on the second type, only the first type AJDE will be discussed in this document.

To illustrate the effect of the 'efficiency' of the jet-diffuser, η_{dj}, on the ejector performance, tests have been conducted with fixed geometric and thermodynamic parameters (and thus fixed η_N, C_{di}, C_{fdj}, α_∞ and $\dot{m}_d/\dot{m}_p$) while varying the size of the end plate. Since the flat ends with zero divergence cannot support the pressure gradient across the diffuser jet, removal or reduction in size of the end plate would seriously collapse the flow pattern within the diffuser, and cause premature termination of the mixing process, which has a direct effect on the parameter η_{dj}. Measurements of thrust augmentation (ϕ) were made for each end plate configuration and plotted vs the length of the end plate as shown on Figure 5 for a diffuser area ratio of 3.

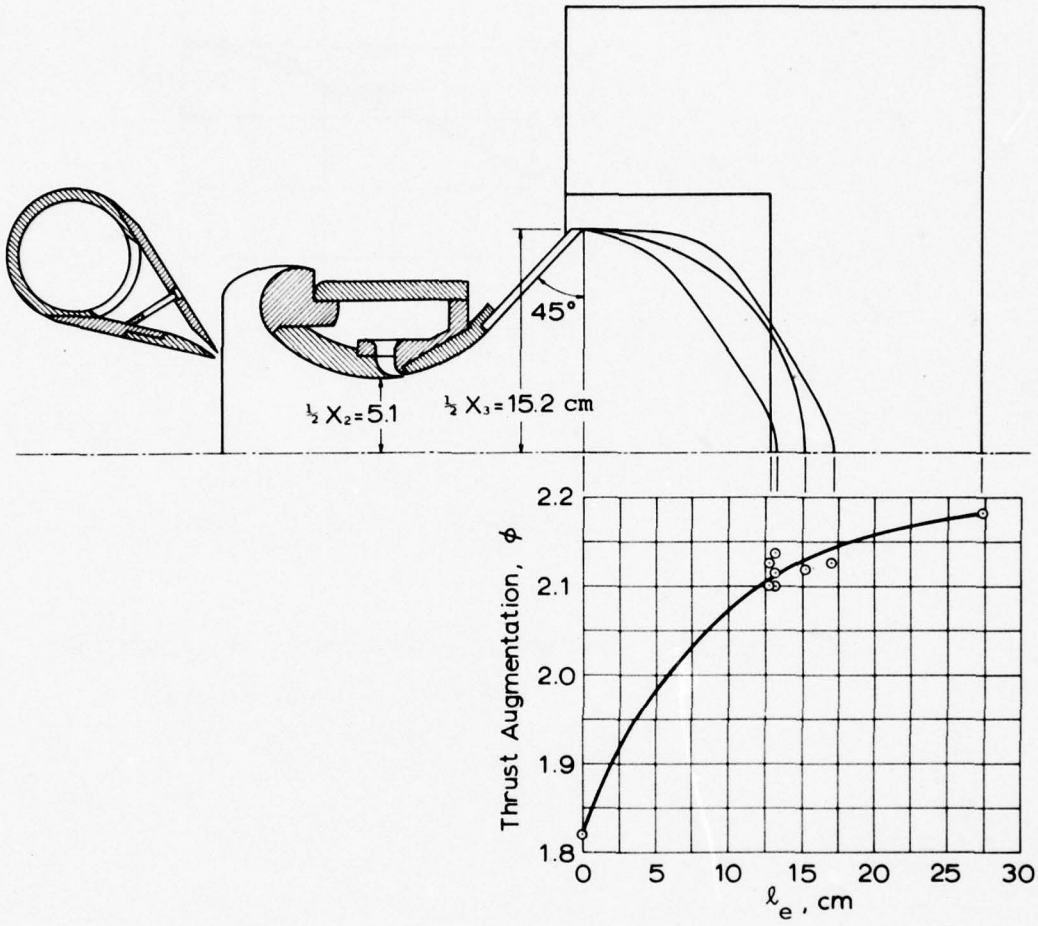

P_o = 24.3 kilopascals (3.52 psig)

$A_2/(s_\infty + a_\infty)$ = 21.6; s_∞/a_∞ = 0.62

Figure 5. END PLATE CONFIGURATIONS AND PERFORMANCE, STAMP EJECTOR

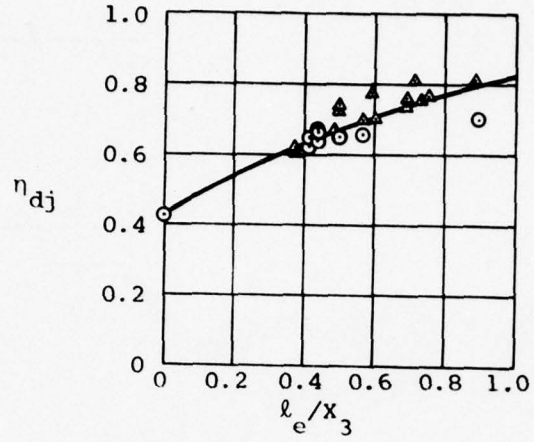

Figure 6. JET-DIFFUSER EFFICIENCY, STAMP EJECTOR

P_o= 24.3 kilopascals (3.52 psig)

$A_2/(s_\infty+a_\infty)$ = 21.6; s_∞/a_∞ = 0.62

This ejector experiment was conducted in air. The Reynolds Number of the diffuser jet Re_{ℓ} was estimated from a compressible equation, and the coefficient of skin friction for the diffuser jet, C_{fdj}, was calculated from Equations 143 and 144, with correction for compressibility effect. Using the method described by Equations 128-134, the value of η_{dj} was calculated and plotted as a function of ℓ_e/X_3 on Figure 6 for a variety of diffuser area ratio from 1.6 to 3.1. As illustrated, the value of η_{dj} is approaching 1.0 as the end plate length increases. This is indicative of the adverse influence of the three-dimensionality of the finite aspect ratio ejector. For larger aspect ratio ejectors, η_{dj} can be expected to be closer to 1. Further improvement of the design technology such as the type 2 AJDE, can also increase this parameter.

It is important to note that the parameter η_{dj} includes the effect of incomplete mixing, which depends on Reynolds Number and the design of the primary nozzle. Experimental data given by Reference 1 indicate that higher ejector performance can be obtained at higher plenum pressure (or higher Reynolds Number) which corresponds to the improvement of η_{dj}.

V DISCUSSION OF EJECTOR PERFORMANCE

1. Parameters

The relative merits of ejector thrusters in comparison to free jets are evaluated in terms of the thrust augmentation (ϕ), the relative power (R_p) and the propulsive efficiency (η_{ej}).

These three parameters are utilized to describe ejector performance since each has a distinct significance and provides essential information.

Thrust augmentation (ϕ) is the most commonly used parameter in ejector technology. As its name implies, ϕ is the ratio of the net thrust available from an ejector, compared to the ideal net thrust of a free jet which is powered by the same machinery as that which supplies the energized fluid to the ejector. Thus if it is desired to obtain an increase of thrust for an existing system, the value of ϕ as a function of ejector geometry at any given operational and power supply characteristics provides the required information.

Ejectors can be used most effectively if the entire propulsive system is designed for use with the ejector. In other words, the optimal use of ejector thrusters requires that the mass flow and head of the pump and the ejector geometry be selected to produce the required thrust over the range of operating conditions, with minimal required jet power.

A useful parameter for this type of design consideration is the relative power (R_p), which is the ratio of required ejector power to the power required to drive a free jet having net thrust equal to the net thrust of the ejector, and whose mass flow through the pump is equal to that passing through the ejector's pump.

Selection of pump characteristics and ejector geometry for minimization of R_p will thus result in an ejector thruster requiring minimal power, for a jet propelled system.

The relationship between thrust augmentation and relative power is significantly different from linear. In fact, relative power can vary approximately as the inverse square of the thrust augmentation and depends weakly on the average pump inlet velocity ratio ($U_p/V_{j\infty}$), as shown on Figure 7.

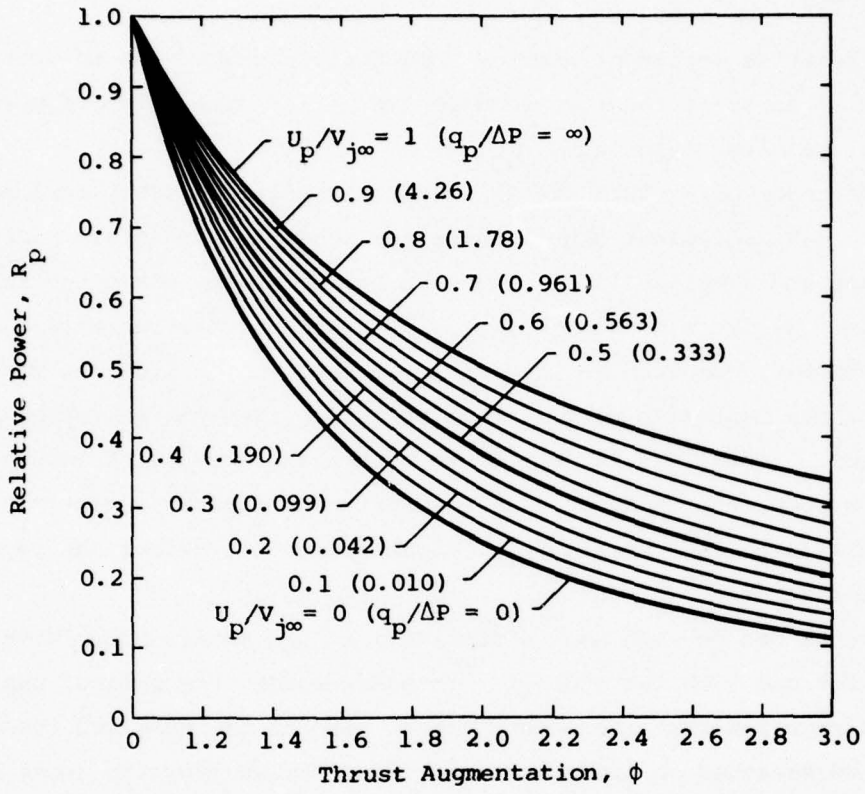

Figure 7. COMPARISON OF EJECTOR/FREE JET POWER REQUIREMENTS

The propulsive efficiency (η_{ej}) of an ejector is the product of the propulsive efficiency (η_{ref}) of a free jet, operating with identical machinery, times the thrust augmentation ϕ of the ejector. With ϕ greater than 1.0, the propulsive efficiency of the ejector always exceeds that of its (reference) free jet.

The relationship among η_{ref}, $q_\infty/\Delta P$, and U_p/U_∞ is illustrated on Figure 8, and can be utilized in estimating the value of η_{ej} from the data presented in the next section.

Comparison of ejector or free jet thrusters to propeller thrusters is somewhat more complex since their power supply machinery and transmission systems are very different. Thus the internal machinery losses and the size and weight of the components must be considered in detail to obtain a realistic comparison of the merits of the ejector vs the propeller. This detailed component comparison is beyond the scope of this study, since it can only be accomplished for a given vehicle system whose requirements of machinery size, fuel capacity, external protrusion, total thrust, etc. are known.

Generally, the designers of a given vehicle can use the propulsive efficiency to make the required comparison of the overall system.

In comparing ejectors with propellers, it is important to note that while the propeller must be circular, the ejector can be tailored to conveniently fit the vehicle contours or to minimize the external protrusion. This also provides a means for maximum utilization of boundary layer fluid for propulsion purposes, the advantage of which will become evident in the following discussions.

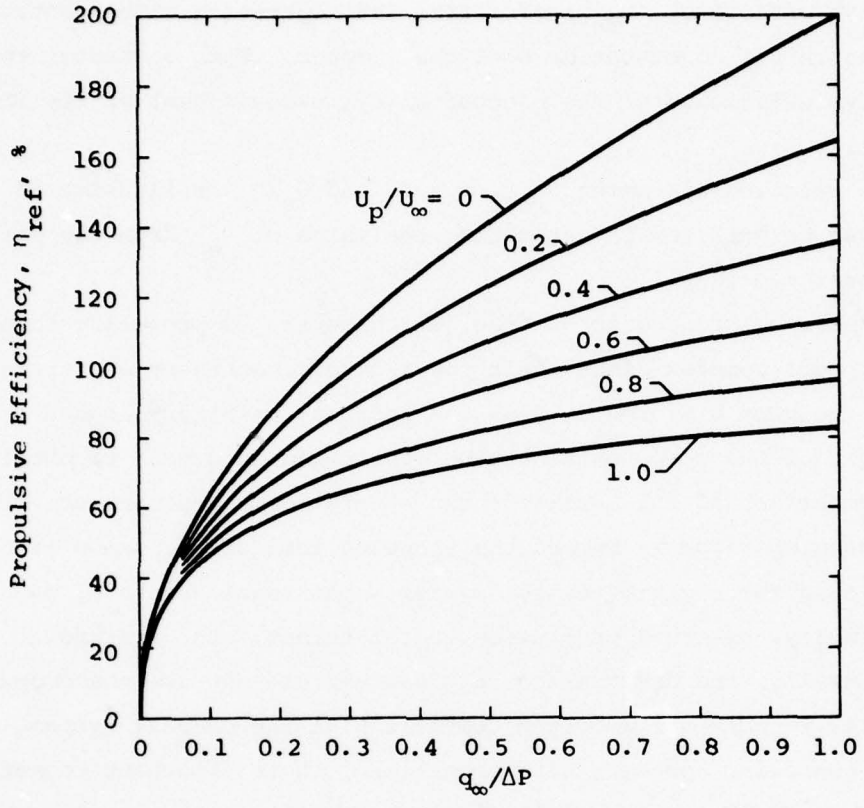

Figure 8. REFERENCE JET PROPULSIVE EFFICIENCY

2. Jet-Diffuser Ejectors

The performance of an ejector depends upon a large number of parameters which are required to describe the environment, the operational, the geometric and power supply characteristics, the losses attributable to the ejector and the performance limitations and optimization conditions. The major obstacles to the use of ejectors as underwater thrusters relate to their size and the difficulty encountered in the minimization of the losses of performance due to drag forces associated with the ejector. The large reduction in ejector size and the associated improvement in performance achievable by the use of a jet-diffuser (a diffuser comprised of a fluid jet) for recovery of jet kinetic energy has been a major influence in the renewed interest in ejectors.

The large reduction in ejector size achieved by the use of jet-diffusion placed emphasis upon the influence of losses due to inlet blockage, skin friction and incomplete mixing of primary and induced flows, on the performance of these ejectors. The analysis described in the previous section of this document has attempted to answer these questions and the following information is intended to present some sample performance data to illustrate the relative importance of various loss factors, and other design parameters.

Most generally, the performance of an ejector having a given geometric size depends upon the ratio of $q_\infty (=1/2\rho U_\infty^2)$ to the pump pressure head (ΔP), as described in the analysis presented in the previous section. A particular example is illustrated on Figure 9 where thrust augmentation is plotted vs $q_\infty/\Delta P$ for an ejector whose geometric parameters are stated on the chart. This generalized performance does not consider limitations imposed by cavitation or losses other than the intrinsic loss of mechanical energy resulting from the mixing process.

The rapid decrease in thrust augmentation with increasing values of $q_\infty/\Delta P$ is fundamental to ejector thrusters and indicates the desirability of operating at small values of $q_\infty/\Delta P$, regardless of speed, depth and other conditions, except as influenced by the losses. The magnitude of the thrust augmentation obviously depends upon the geometric parameters which are fixed in the example illustrated on Figure 9, and upon the characteristics of the ingested fluid which on Figure 9 are assumed to be free-stream fluid, at an arbitrary depth.

It is important to note that the jet-diffuser ejector can provide ideal performance virtually equivalent to the more conventional but larger solid diffuser ejector, over most of the range of values of $q_\infty/\Delta P$. The performance of the jet-diffuser ejector depends upon the choice of mass flow ratio $\dot{m}_d/\dot{m}_p$ in addition to the other geometric quantities, as illustrated.

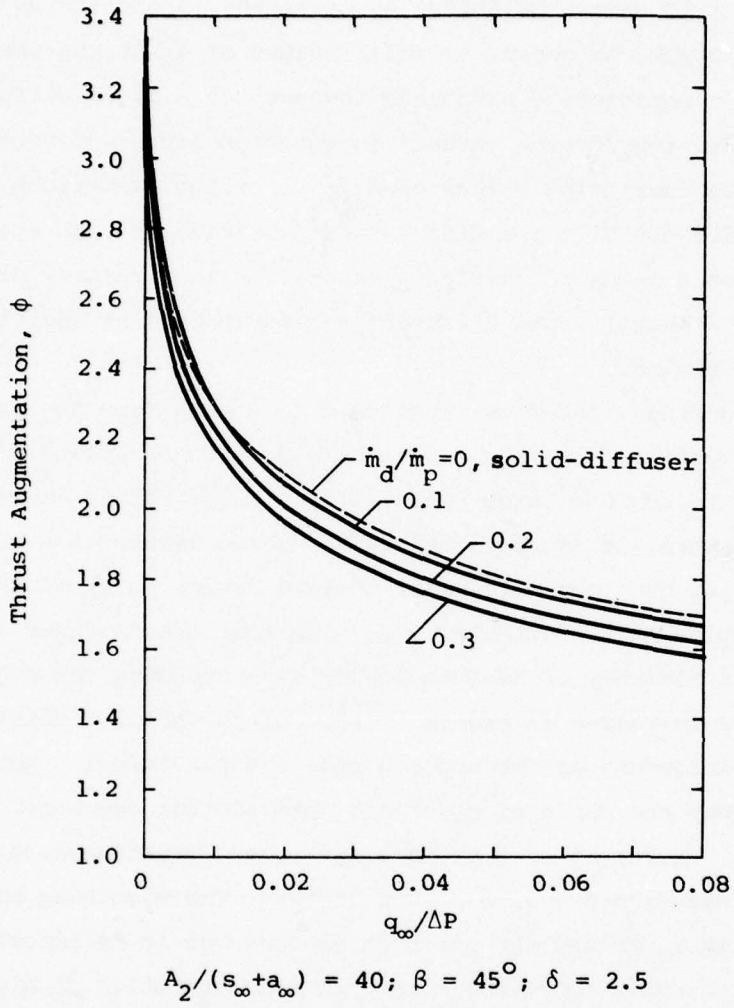

Figure 9. IDEAL THRUST AUGMENTATION OF TRANSLATING JET-DIFFUSER EJECTOR

A more detailed understanding of the influence of $\dot{m}_d/\dot{m}_p$ can be obtained from Figure 10 where the thrust augmentation is plotted vs $\dot{m}_d/\dot{m}_p$ for several values of $q_\infty/\Delta P$. As shown, at small values of $q_\infty/\Delta P$ the use of $\dot{m}_d/\dot{m}_p > 0$ can result in a performance advantage compared to a solid diffuser ejector. At high values of $q_\infty/\Delta P$ the thrust augmentation decreased monotonically but slowly with increasing values of $\dot{m}_d/\dot{m}_p$, for the conditions used in this example. The use of a jet-diffuser is justified at high speeds however, since it provides a means for avoiding separation in a rapidly diverging (and therefore a short) solid diffuser, and for providing additional length for effective mixing.

The diffuser jet flow is assumed to emerge from the end of the solid diffuser surface at an angle β with respect to the plane of symmetry of the ejector. To achieve large solid diffuser area ratios and avoid excessively long structure, it is essential to use large values of β and to utilize the diffuser jet as a boundary layer control device to avoid separation in the solid portion of the diffuser. In addition, the diffuser jet can provide additional recovery of kinetic energy by increasing the effective diffuser area ratio to values in excess of that of the solid diffuser.

The influence of the angle β upon ejector thrust augmentation also depends upon the ratio of $q_\infty/\Delta P$ and upon ejector geometry. As shown on Figure 11, increases of β produce increased thrust augmentation over the entire range from $\beta = 0$ to $\beta = 90$ degrees. The magnitude of the influence of β varies with $q_\infty/\Delta P$ and the other parameters but it is important to note that despite the small improvement in thrust augmentation at high speed, the use of large values of β provides the additional, important advantage of extending the region of sub-ambient pressure which can be effectively utilized for mixing. A more realistic but still general evaluation of the jet-diffuser ejector can be obtained by a comparison of its performance at a given speed at the limit imposed by cavitation.

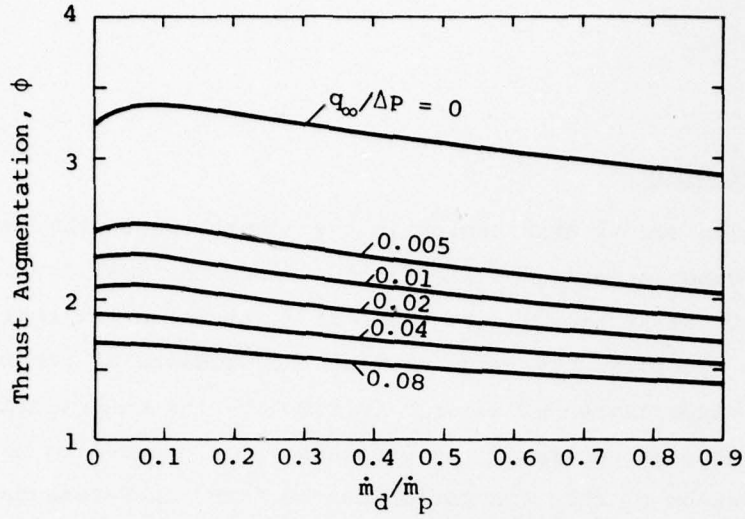

$U_\infty = U_p = U_e$; $A_2/(s_\infty + a_\infty) = 40$; $\beta = 45^o$; $\delta = 2.5$

Figure 10. INFLUENCE OF DIFFUSER/PRIMARY MASS FLOW RATIO ON THRUST AUGMENTATION

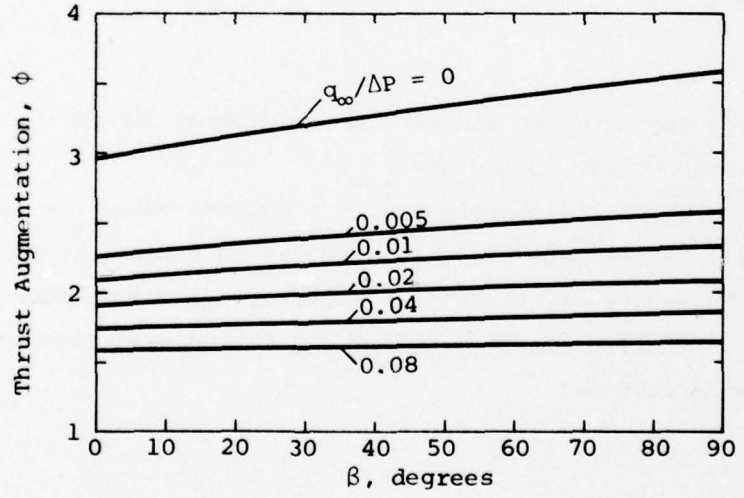

$U_\infty = U_p = U_e$; $A_2/(s_\infty + a_\infty) = 40$; $\dot{m}_d/\dot{m}_p = 0.2$; $\delta = 2.5$

Figure 11. INFLUENCE OF DIFFUSER EXIT ANGLE ON THRUST AUGMENTATION

3. Cavitation Limit

Cavitation occurs at a region in the ejector where the local pressure reaches the vapor pressure of the fluid. Since the smallest pressure in an ejector occurs at Station 1, the value of λ_1 at which cavitation is initiated can be determined by assuming that the pressure at Station 1 is the pressure of vaporization of water. To simplify the mathematics and without significant loss of accuracy, the pressure p_1 is assumed to be zero. Detailed discussion of this assumption can be found in Reference 2.

Assuming $p_1 = 0$, then

$$\lambda_{1,c} = \frac{U_1}{V_{p_1}} = \sqrt{\frac{p_\infty/\Delta P_{eff} + q_e/\Delta P_{eff}}{(1 + C_{di})\ [1 + p_\infty/\Delta P_{eff} + q_e/\Delta P_{eff}]}}$$

and the thrust augmentation can then be calculated for an ejector operating at its cavitation limit, using $\lambda_1 = \lambda_{1,c}$.

Since the ejector's performance is a maximum when $\lambda_1 = \lambda_{1,c}$, performance data will be evaluated at this critical condition. To provide design information necessary to obtain this value of λ_1, the diffuser area ratio required for operation at the limit of cavitation will also be presented on the performance curves.

4. Real Fluid Effects on Ejector Performance

a) Primary jet

The real fluid effects on ejector performance can be evaluated by the use of the efficiency and loss factors as described in the analysis. It is essential that values given to these loss parameters be consistant with the manner in which they are defined. For example, the nozzle efficiency is defined as the ratio of the momentum resulting from an expansion of the primary jet fluid from the stagnation pressure to ambient pressure with nozzle losses to the momentum resulting from the same expansion without loss. This important parameter has a large influence on ejector performance since the thrust augmentation varies directly with nozzle efficiency, the relationship being linear at small values of $q_\infty/\Delta P$.

b) Diffuser jet

Diffuser jet losses are comprised of the loss of momentum due to skin friction on the surface of the solid diffuser and of a departure from the ideal case attributable to incomplete mixing and three-dimensional effects. The influence of skin friction is accounted for by evaluation of the coefficient C_{fdj} as a function of Reynolds Number using the appropriate law depending upon whether the flow is laminar or turbulent, as discussed in Section IV. The loss due to incomplete mixing is virtually non-existent in a properly designed jet-diffuser since the mixing process can continue for a considerable distance downstream of the solid surfaces where the pressure remains sub-ambient due to the jet-diffuser process. Three-dimensional effects however can limit the extent of the jet-diffuser in a streamwise direction and may be responsible for a reduction in the value of η_{dj} below 1.0.

Tests of stationary ejectors at FDRC have indicated that despite a relatively poor design (flat ends) on the ends of this low aspect ratio rectangular ejector, the value of η_{dj} approached 0.8. The jet-diffuser efficiency can approach 1.0 if the ejector has a higher aspect ratio and the solid surfaces of the diffuser are carefully designed.

The influence of jet-diffuser efficiency on thrust augmentation is described on Figure 12, for non-cavitating ejectors. This chart illustrates the fact that smaller values of η_{dj} result in a requirement for larger solid diffuser area ratios. The larger solid diffuser area ratios involve more skin friction and therefore the net result is a decrease in performance resulting from the increased diffuser losses.

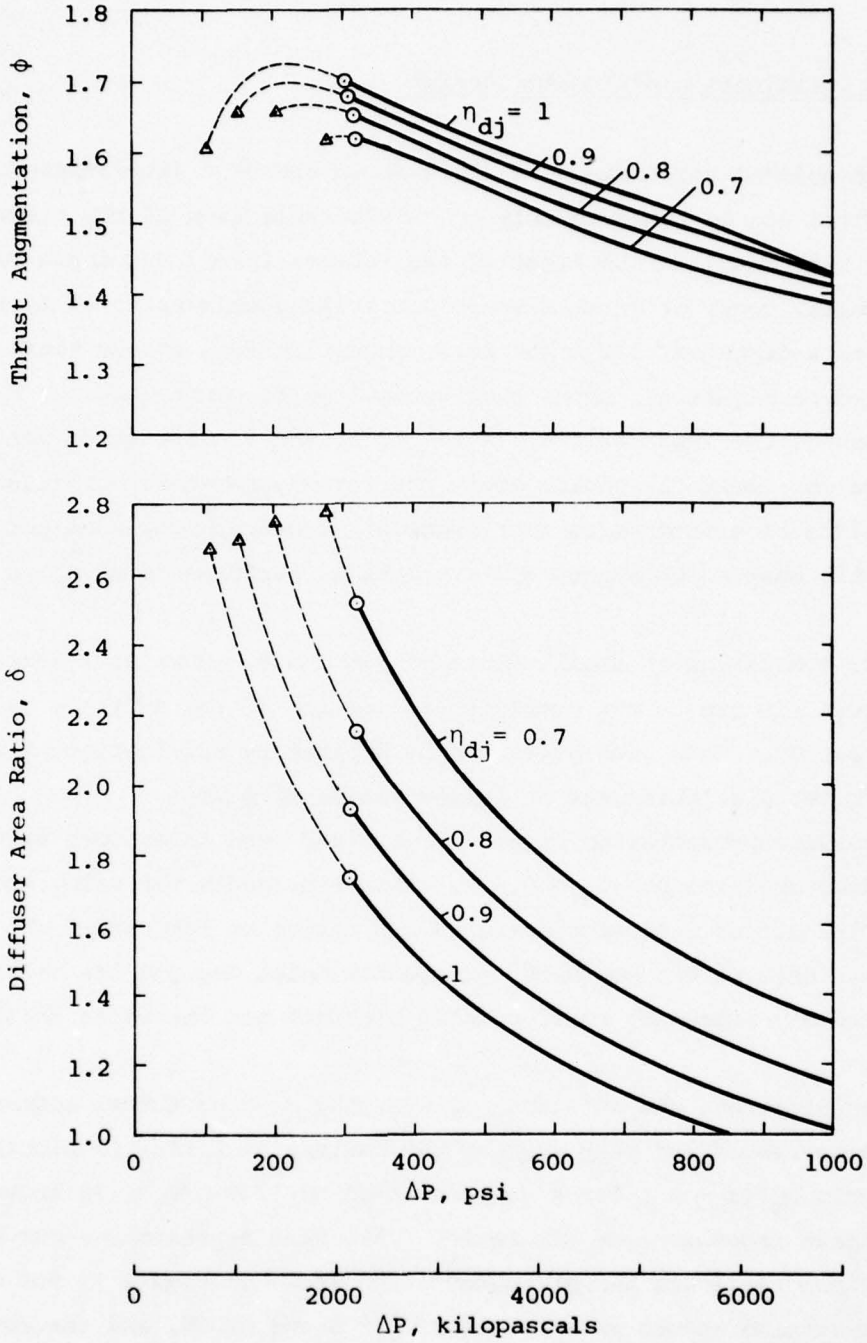

$U_\infty = U_p$ = 12.9 m/sec (25 knots); U_e/U_∞ = 0.5;
Depth = 15.2 m (50 feet);
X_2 = 10.2 cm (4 in.); $\beta = 45^o$; $\dot{m}_d/\dot{m}_p$ = 0.2;
$A_2/(s_\infty + a_\infty)$ = 40; η_N = 1; C_{di} = 0.01;
$C_{fdj} = fn(Re_\ell)$

Figure 12. INFLUENCE OF JET-DIFFUSER EFFICIENCY ON THRUST AUGMENTATION

c) Optimization of Ejector Design

The optimal performance of any ejector and of a jet-diffuser ejector in particular, can be achieved only by careful selection of the ejector geometry and the pump head, in the light of the vehicle speed, and depth of operation. For example, consider first a vehicle traveling at a speed of 12.9 m/sec (25 knots) at a depth of 15.2 m (50 ft.), ingesting free-stream fluid. The data presented on Figure 13, shows that optimal performance requires a careful selection of the area ratio $A_2/(s_\infty + a_\infty)$, ΔP and δ. Specified vehicle constraints can limit the choice among the three parameters but regardless of limitations of ejector size (for example), a proper pump head and diffuser area ratio must be chosen to achieve optimal performance as shown on Figure 13.

The limitation at small values of pump head, shown as a termination of the curves, is due to the complete dissipation of the diffuser jet due to skin friction. This limitation can be avoided by utilization of the larger diffuser jet slot thickness or larger values of $\dot{m}_d/\dot{m}_p$.

The data presented on Figure 13 is based upon an assumed value of the inlet drag coefficient ($C_{di} = 0.01$). This represents the value encountered by the jet-diffuser ejector designed and tested at FDRC under the STAMP Program. More recent concepts for ejector inlet designs are being investigated and may represent smaller inlet blockage and therefore smaller values of C_{di}.

To illustrate the influence of C_{di}, the maximum thrust augmentation, and the corresponding pump head at the cavitation limit, is plotted vs the area ratio $A_2/(s_\infty + a_\infty)$ for a vehicle speed of 12.9 m/sec (25 knots) with free-stream ingestion, on Figure 14. This data represents a curve through the maximum realistic thrust augmentation shown on Figure 13 for $C_{di} = 0.01$. Similar considerations were made for $C_{di} = 0$ and 0.005, and the results are shown plotted on Figure 14 for comparison.

At higher speeds the inlet drag coefficient has a more pronounced effect on the thrust augmentation. For example on Figure 15, at a speed of 25.7 m/sec (50 knots), the thrust augmentation at the cavitation limit is plotted vs the area ratio for the same range of values of C_{di}.

Significant improvement in ejector performance can be achieved by the ingestion of boundary layer fluid as discussed in the following section.

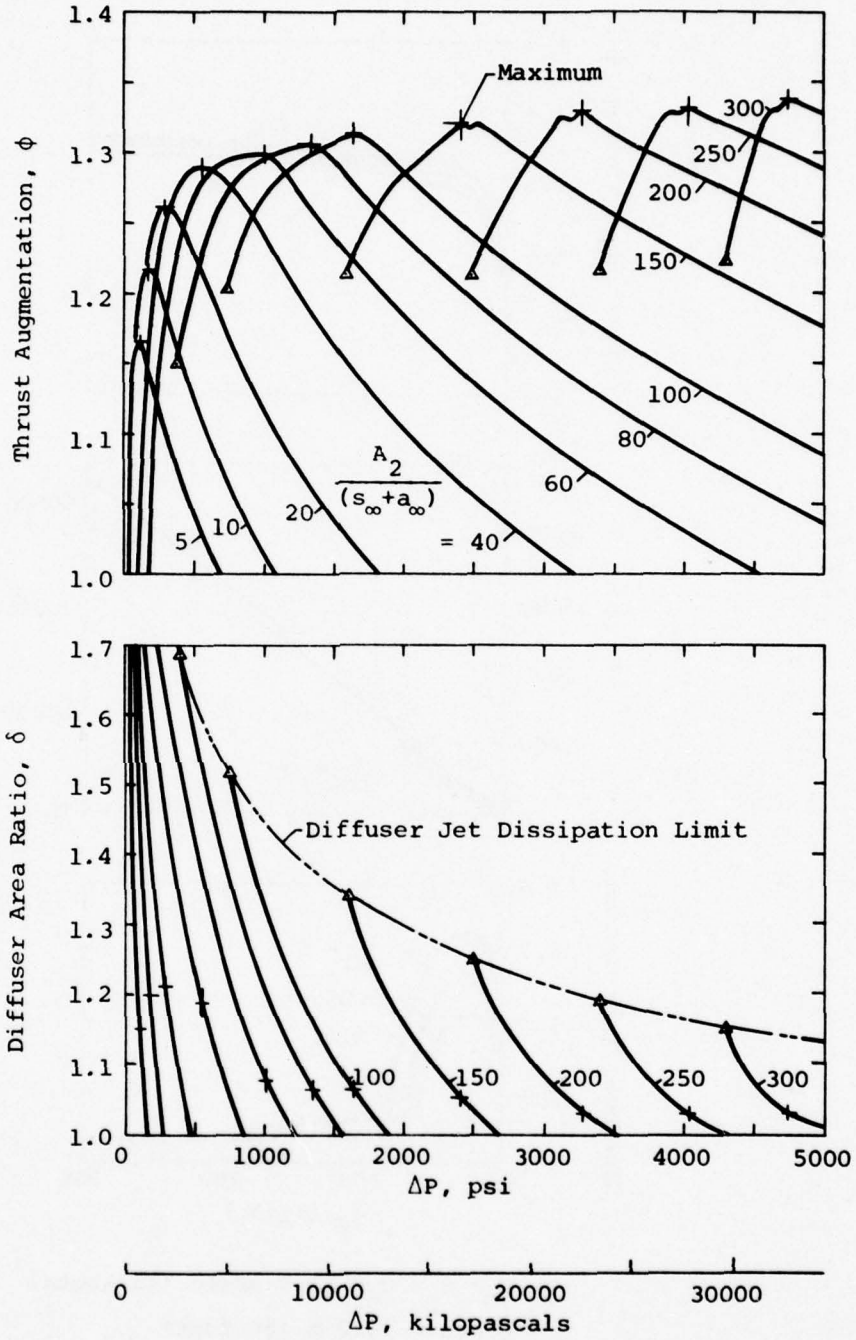

$U_\infty = U_p = U_e = 12.9$ m/sec (25 knots);
Depth = 15.2 m (50 feet);
$X_2 = 10.2$ cm (4 in.); $\beta = 45^o$
$\eta_N = \eta_{dj} = 1$; $C_{fdj} = fn(Re_\ell)$;
$C_{di} = 0.01$; $\dot{m}_d/\dot{m}_p = 0.2$

Figure 13. OPTIMIZATION OF JET-DIFFUSER EJECTORS WITH INLET IN FREE-STREAM

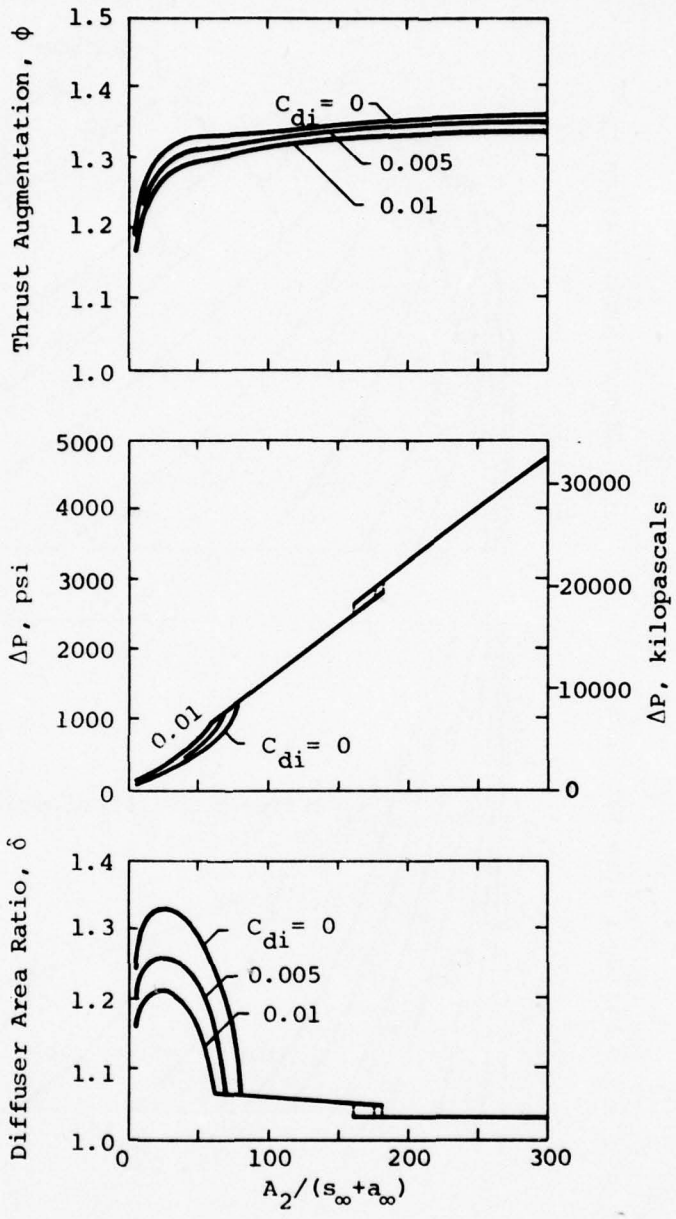

$U_\infty = U_p = U_e$ = 12.9 m/sec (25 knots)

Depth = 15.2 m (50 feet)

X_2 = 10.2 cm (4 in.); $\beta = 45^o$

$\eta_N = \eta_{dj} = 1$; $C_{fdj} = fn(Re_\ell)$

$\dot{m}_d/\dot{m}_p = 0.2$

Figure 14. OPTIMUM PERFORMANCE OF JET-DIFFUSER EJECTORS WITH INLET IN FREE-STREAM (12.9 m/sec)

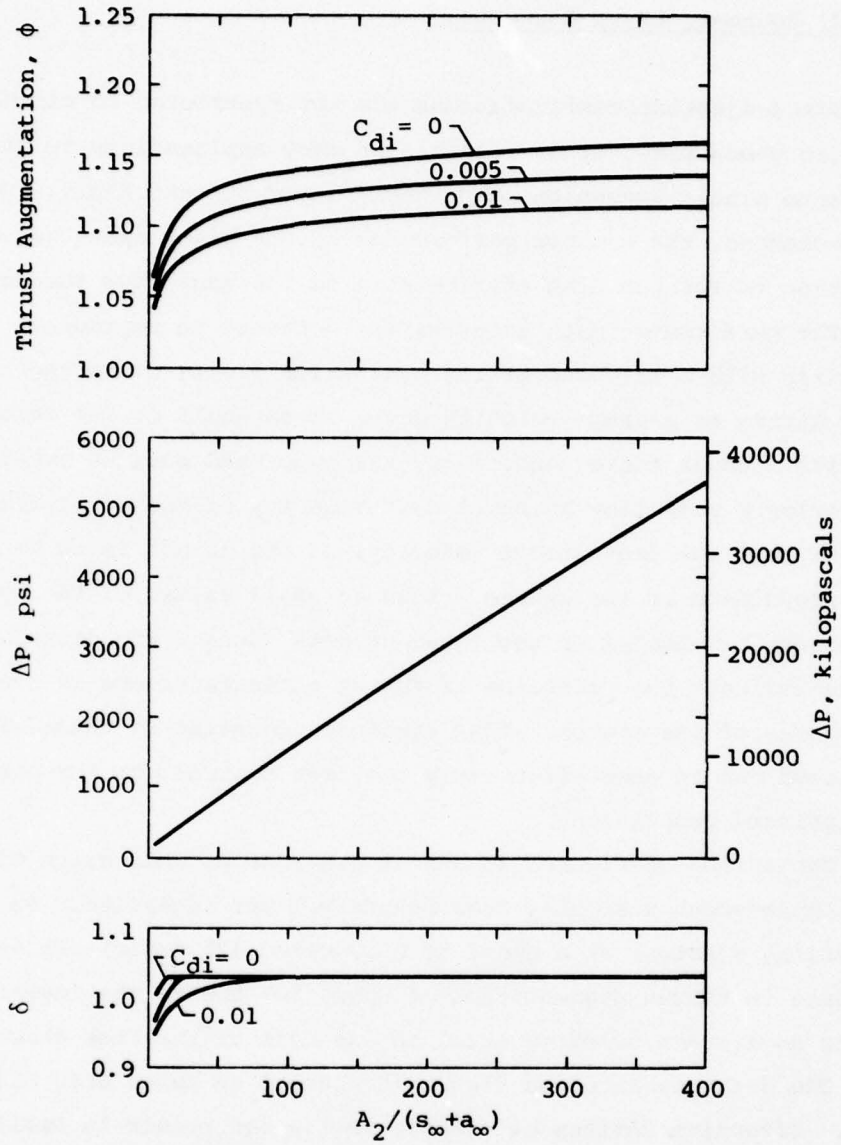

$U_\infty = U_p = U_e$ = 25.7 m/sec (50 knots);
Depth = 15.2 m (50 feet);
X_2 = 10.2 cm (4 in.); $\beta = 45^\circ$;
$\eta_N = \eta_{dj} = 1$; $C_{fdj} = fn(Re_\ell)$
$\dot{m}_d/\dot{m}_p = 0.2$

Figure 15. OPTIMUM PERFORMANCE OF JET-DIFFUSER EJECTORS WITH INLET IN FREE-STREAM (25.7 m/sec)

d) Boundary Layer Ingestion

Since ejectors configurations are not restricted to circular or axi-symetric geometries, it is feasible in many applications to distribute their inlets to enable ingestion of boundary layer or wake fluid. Under these circumstances, the ejector performance at any given speed can be improved by reduction of the ram drag attributable to the mass flow through the ejector.

The performance data illustrated on Figure 16 represents an ejector operating with a diffuser at its cavitation limit, ingesting boundary layer fluid having an average velocity equal to one-half of the free-stream velocity. Under these conditions, the pump head must be sufficiently large to provide a mass flow averaged exit velocity of the total fluid equal to or greater than the free-stream velocity, if the thrust is to be sufficient for self-propulsion of the system. Thus at small values of the pump head, the curves are terminated or continued as dash lines. The dashed portion of the curves indicate the existence of thrust whose magnitude is smaller than the total drag of the system. Thus ejectors operating at these small values of pump head can be used effectively only for control, or for purposes other than primary propulsion.

Comparison of Figures 13 and 16 provides an indication of the performance improvement resulting from boundary layer ingestion. As shown, self-propelling ejectors at a speed of 12.9 m/sec (25 knots) can achieve an increase in thrust augmentation of about 30% due to the ingestion of fluid having an average velocity equal to one-half of the free stream velocity.

The data presented on Figure 16 assumed an inlet drag coefficient C_{di} = 0.01. Effective designs of ejector inlets can result in smaller values of the inlet drag.

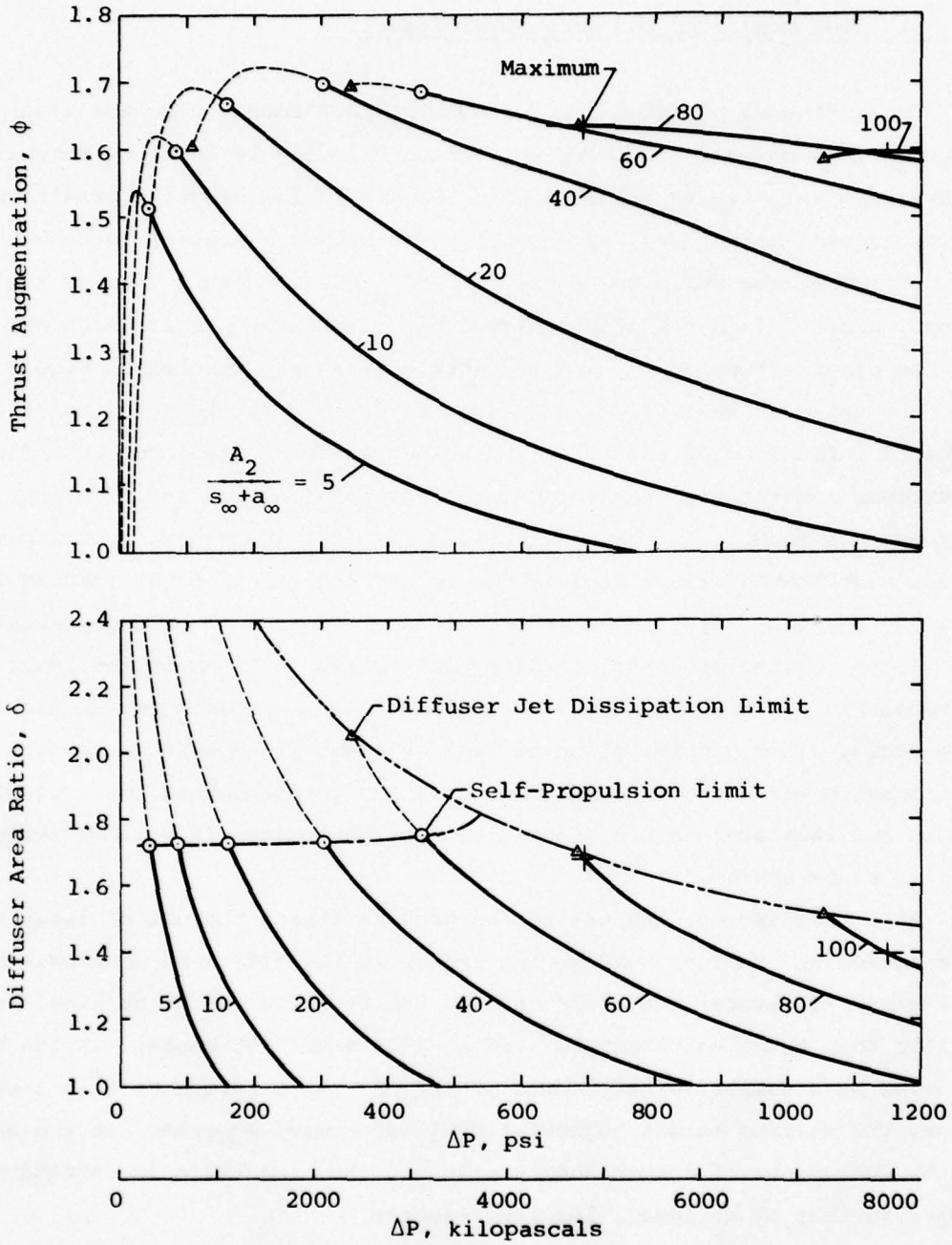

$U_\infty = U_p = 12.9$ m/sec (25 knots); $U_e/U_\infty = 0.5$;
Depth = 15.2 m (50 feet);
$X_2 = 10.2$ cm (4 in.); $\beta = 45^\circ$; $\dot{m}_d/\dot{m}_p = 0.2$;
$\eta_N = \eta_{dj} = 1$; $C_{fdj} = fn(Re_\ell)$; $C_{di} = 0.01$

Figure 16. OPTIMIZATION OF JET-DIFFUSER EJECTORS WITH INLET IN BOUNDARY LAYER

e) Inlet Drag with Boundary Layer Ingestion

The influence of inlet drag on ejector performance when the ejector inlet is in a boundary layer whose average velocity is equal to one-half the free-stream velocity is illustrated on Figure 17 for specific conditions of vehicle speed, depth, etc, as shown. These curves represent the envelope through the maxima shown on Figure 16 for C_{di}= 0.01 within various limitations, discussed in the previous section. Similar considerations were made for the other values of C_{di} and the envelopes also presented on Figure 17.

The unusual shape of the curves on Figure 17 are the result of the combined influences of the inlet and skin friction losses and the influence of various limitations (cavitation, self-propulsion, and insufficiency of diffuser jet flow). As the area ratio $A_2/(s_\infty+a_\infty)$ increases, initally the thrust augmentation rises rapidly due to the ingestion of the induced flow from the boundary layer. Further area ratio increases to values greater than 60, limits the use of large diffuser area ratios as shown on the lower curve of Figure 16. Therefore the augmentation decreases despite increased area ratio. Thus consideration of real, viscous fluid effects results in an optimization which is very different from the corresponding ideal considerations and indicates that ejector size must be limited if maximum performance is to be achieved.

At higher speeds, the cavitation problem limits the use of large diffuser area ratios and thereby reduces the losses in the diffuser. For example, at 25.7 m/sec (50 knots) the diffuser area ratios which can be utilized are smaller than those which can be used at 12.9 m/sec (25 knots), as can be observed by a comparison of Figure 17 and 18. As a result of this limitation, the maximum thrust augmentation is decreased somewhat but the nature of the dependence of thrust augmentation on the area ratio is considerably closer to that of an ideal, lossless ejector.

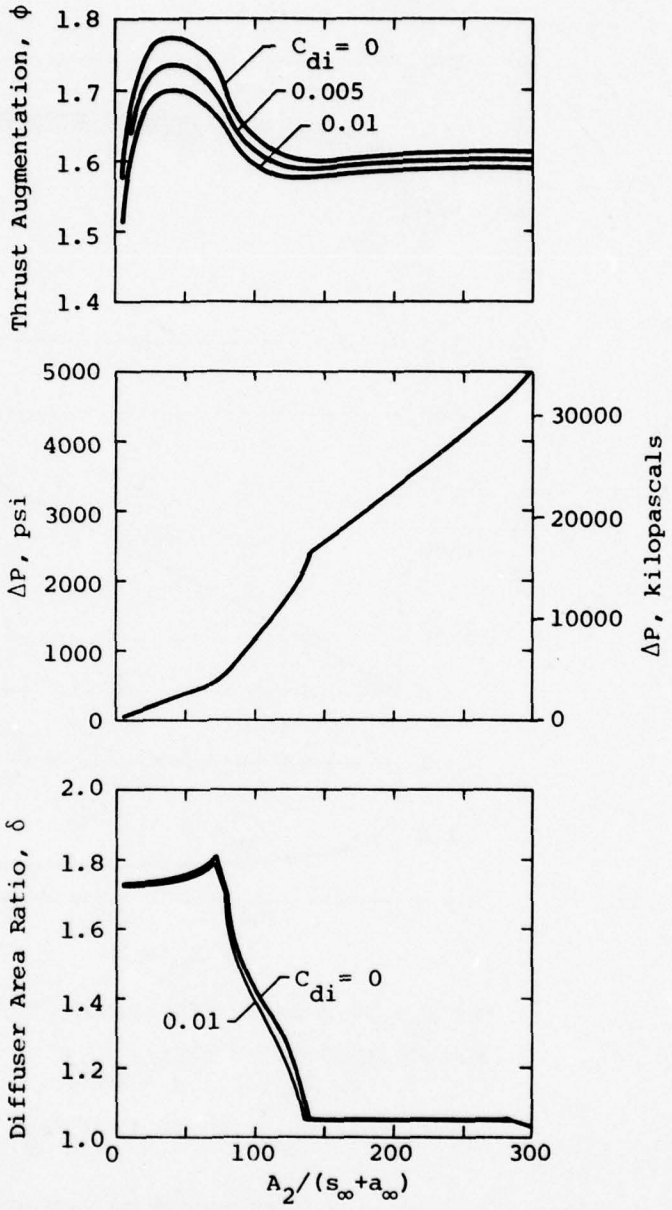

$U_\infty = U_p = 12.9$ m/sec (25 knots); $U_e/U_\infty = 0.5$

Depth = 15.2 m (50 feet);

$X_2 = 10.2$ cm (4 in.); $\beta = 45^o$; $\dot{m}_d/\dot{m}_p = 0.2$

$\eta_N = \eta_{dj} = 1$; $C_{fdj} = fn(Re_\ell)$

Figure 17. OPTIMUM PERFORMANCE OF JET-DIFFUSER EJECTORS WITH INLET IN BOUNDARY LAYER (12.9 m/sec)

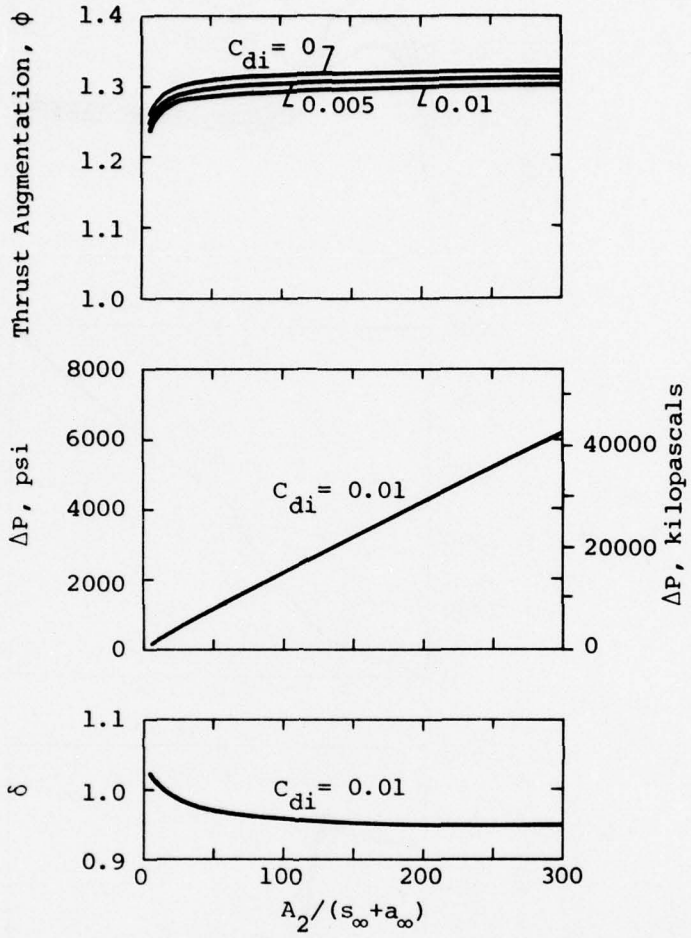

$U_\infty = U_p$ = 25.7 m/sec (50 knots); U_e/U_∞ = 0.5

Depth = 15.2 m (50 feet);

X_2 = 10.2 cm (4 in.); $\beta = 45^\circ$;

$\eta_N = \eta_{dj} = 1$; $C_{fdj} = fn(Re_\ell)$; $\dot{m}_d/\dot{m}_p = 0.2$

Figure 18. OPTIMUM PERFORMANCE OF JET-DIFFUSER EJECTORS WITH INLET IN BOUNDARY LAYER (25.7 m/sec)

f) Diffuser/Primary Mass Flow Ratio

Since, for a jet-diffuser ejector, the relative mass flows apportioned between the diffuser and primary jets can influence the effectiveness of the boundary layer control capability of the diffuser jet and the overall performance of the ejector, the thrust augmentation was calculated as a function of $\dot{m}_d/\dot{m}_p$ for speeds of 12.9 m/sec (25 knots) and 25.7 m/sec (50 knots) and for free-stream and boundary layer ingestion.

The ratio of diffuser jet mass flow to primary jet mass flow influences the performance of a jet-diffuser ejector as illustrated on Figure 19 and 20. At a speed of 12.9 m/sec (25 knots), the thrust augmentation is presented as a function of $\dot{m}_d/\dot{m}_p$ for free-stream and boundary layer inlets on Figure 19. As shown, it is necessary to utilize a specific value of $\dot{m}_d/\dot{m}_p$ for optimal performance and this optimal choice depends upon the inlet flow velocity and the inlet drag coefficient. In addition, the influence of the skin frictions along the interface between the diffuser jet and the solid diffuser surface is also illustrated as the difference between the solid and the dashed lines.

At a speed of 25.7 m/sec (50 knots), the optimization of $\dot{m}_d/\dot{m}_p$ takes a form similar to that at the lower speed as shown on Figure 20. However it is important to note that the influences of skin friction at the diffuser jet is less important at the high speed as a result of the requirement for smaller solid diffuser area ratios due to cavitation limit.

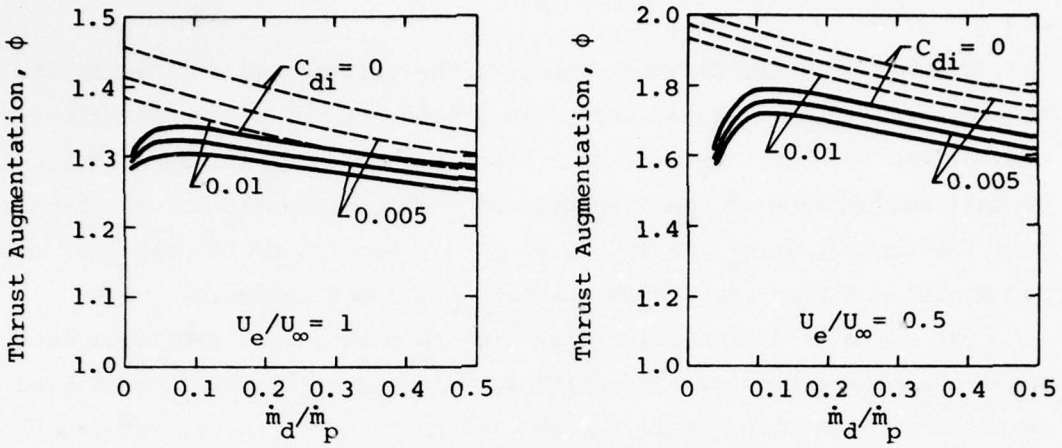

$U_\infty = U_p$ = 12.9 m/sec (25 knots); Depth = 15.2 m (50 feet);
X_2 = 10.2 cm (4 in.); $\beta = 45^o$; $\eta_N = \eta_{dj} = 1$; $A_2/(s_\infty + a_\infty) = 40$
——— $C_{fdj} = fn(Re_\ell)$; ---------- $C_{fdj} = 0$

Figure 19. INFLUENCE OF DIFFUSER/PRIMARY MASS FLOW RATIO AND DIFFUSER JET SKIN FRICTION ON EJECTOR PERFORMANCE (12.9 m/sec)

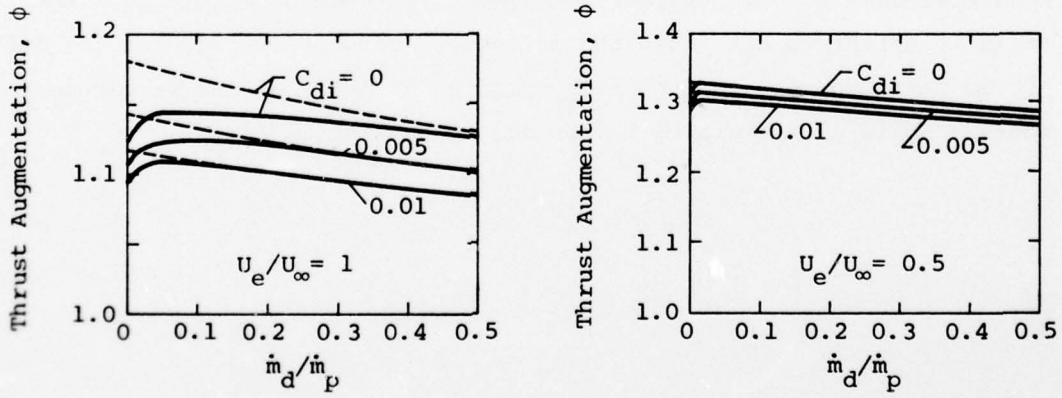

$U_\infty = U_p$ = 25.7 m/sec (50 knots); Depth = 15.2 m (50 feet)
X_2 = 10.2 cm (4 in.); $\beta = 45^o$; $\eta_N = \eta_{dj} = 1$; $A_2/(s_\infty + a_\infty) = 100$;
——— $C_{fdj} = fn(Re_\ell)$; ---------- $C_{fdj} = 0$

Figure 20. INFLUENCE OF DIFFUSER/PRIMARY MASS FLOW RATIO AND DIFFUSER JET SKIN FRICTION ON EJECTOR PERFORMANCE (25.7 m/sec)

g) Depth of Operation

As the depth increases, cavitation occurs at larger values of the diffuser area ratio. The actual values of diffuser area ratios which represent the cavitation limit depend upon the area ratio $A_2/(s_\infty+a_\infty)$, the speed of the vehicle and to some extent the loss coefficients.

To illustrate the advantage of deep submergence, the maximum thrust augmentation is plotted as a function of depth for a range of values of U_e/U_∞. The pump head and cavitation limited diffuser area ratios, at the stated values of the operational, geometric and loss parameters, are also shown on Figure 21. As shown the achievable thrust augmentation increases rapidly with increased depth as a result of the feasibility for use of larger diffuser area ratios.

The influence of the inlet drag coefficient on ejector performance over a range of operating depths is illustrated on Figure 22. As shown the thrust augmentation achievable increases with increasing depth, and decreases with increasing inlet drag.

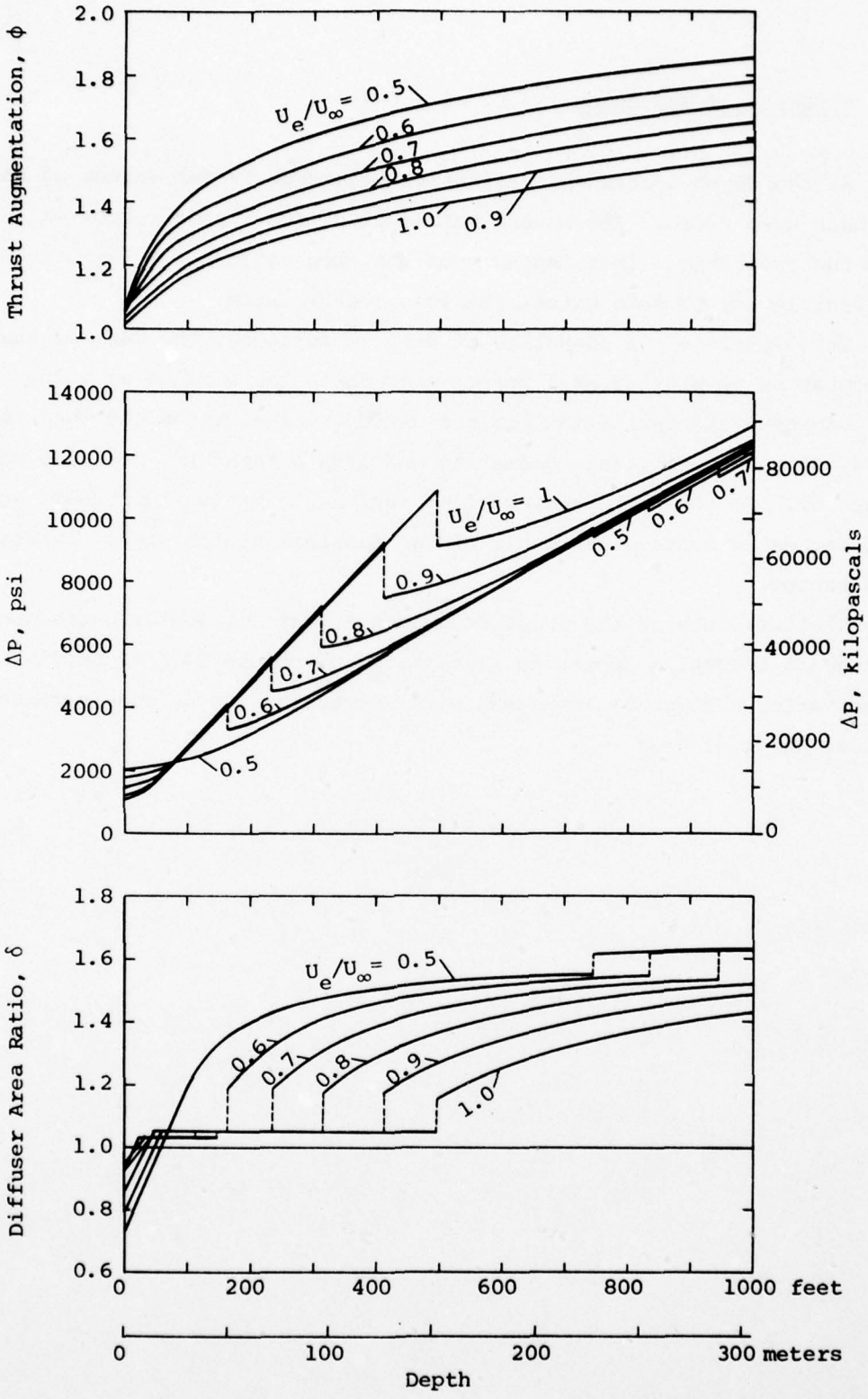

$U_\infty = U_p$ = 25.7 m/sec (50 knots); X_2 = 10.2 cm (4 in.); $\beta = 45^o$;
$A_2/(s_\infty + a_\infty) = 100$; $\dot{m}_d/\dot{m}_p = 0.2$; $C_{di} = 0.01$; $\eta_N = \eta_{dj} = 1$; $C_{fdj} = fn(Re_\ell)$

Figure 21. INFLUENCE OF DEPTH AND BOUNDARY LAYER INGESTION ON EJECTOR PERFORMANCE (25.7 m/sec)

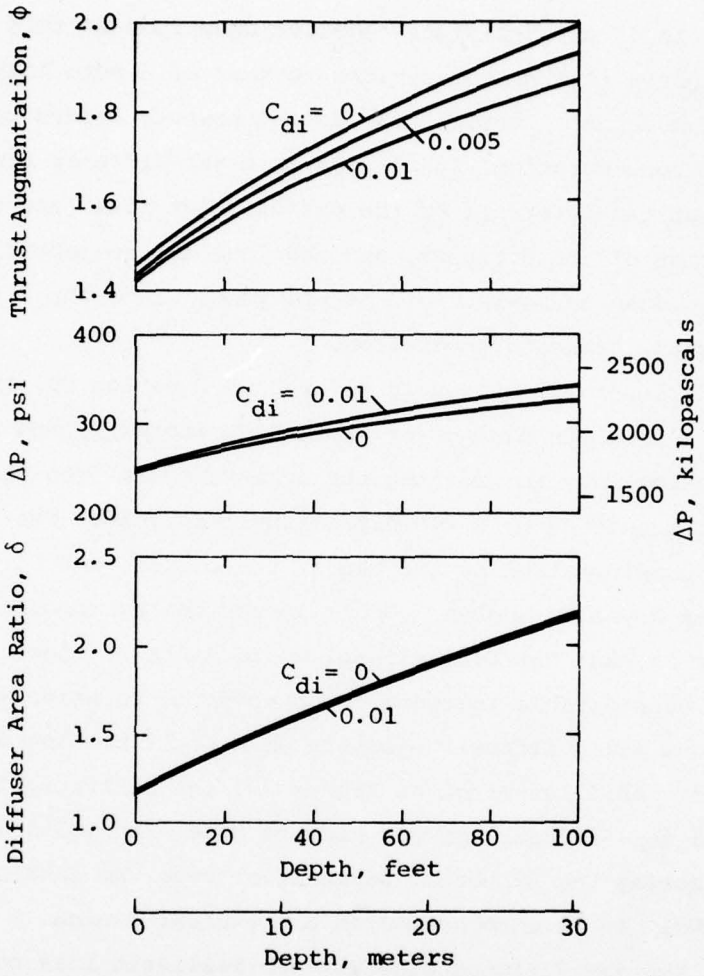

$U_\infty = U_p = 12.9$ m/sec (25 knots); $U_e/U_\infty = 0.5$

$X_2 = 10.2$ cm (4 in.); $\beta = 45^o$;

$A_2/(s_\infty + a_\infty) = 40$; $\dot{m}_d/\dot{m}_p = 0.2$

$\eta_N = \eta_{dj} = 1$; $C_{fdj} = fn(Re_\ell)$

Figure 22. INFLUENCE OF DEPTH AND INLET DRAG ON EJECTOR PERFORMANCE (12.9 m/sec)

5. Comparison of Jet and Solid Diffuser Ejectors

The analysis of a jet-diffuser ejector described in this document has included the losses in a manner similar to that of a more conventional solid diffuser ejector. The diffuser losses however depend upon the type of diffuser under consideration. The losses in a jet-diffuser consist of the skin friction at the interface of the diffuser jet fluid and the surface of the solid portion of the diffuser, and the loss due to incomplete mixing. Flow separation does not exist in a jet-diffuser since the diffuser jet, if properly designed, prevents separation.

The jet-diffuser efficiency as defined by Equation 89, includes the influences of incomplete mixing (or flow non-uniformity) and the influence of three-dimensionality in limiting the achievement of the effective area ratio (σ) predicted by a two-dimensional analysis. The skin friction is taken into consideration by the use of the coefficient C_{fdj} as a function of the Reynolds Number. Other losses can be accounted for in a manner similar to that for conventional solid diffuser ejectors.

It is of considerable interest to observe the relative merits of jet-diffuser and solid diffuser ejectors when realistic losses for each are considered. As illustrated on Figure 23, the realistic thrust augmentation of a jet-diffuser ejector exceeds that of a solid diffuser ejector (neglecting the effect of separation) over the entire range of conditions likely to be encountered in a practical design.

Further, the jet-diffuser ejector with realistic loss coefficients is shown to be capable of providing performance which is only slightly smaller than an ideal solid diffuser ejector over a large range of pump heads and at large pump heads the realistic jet-diffuser ejector performance exceeds that of an ideal solid diffuser ejector. The fact that the performance of the jet-diffuser ejector with losses exceeds that of an ideal solid diffuser ejector is a result of the distribution of injected fluid between the primary and diffuser jet, which causes the inlet area ratio ($\alpha = A_2/a_1$) to be larger for a jet-diffuser ejector than for a solid diffuser ejector whose primary nozzle delivers all injected fluid at the throat of the ejector.

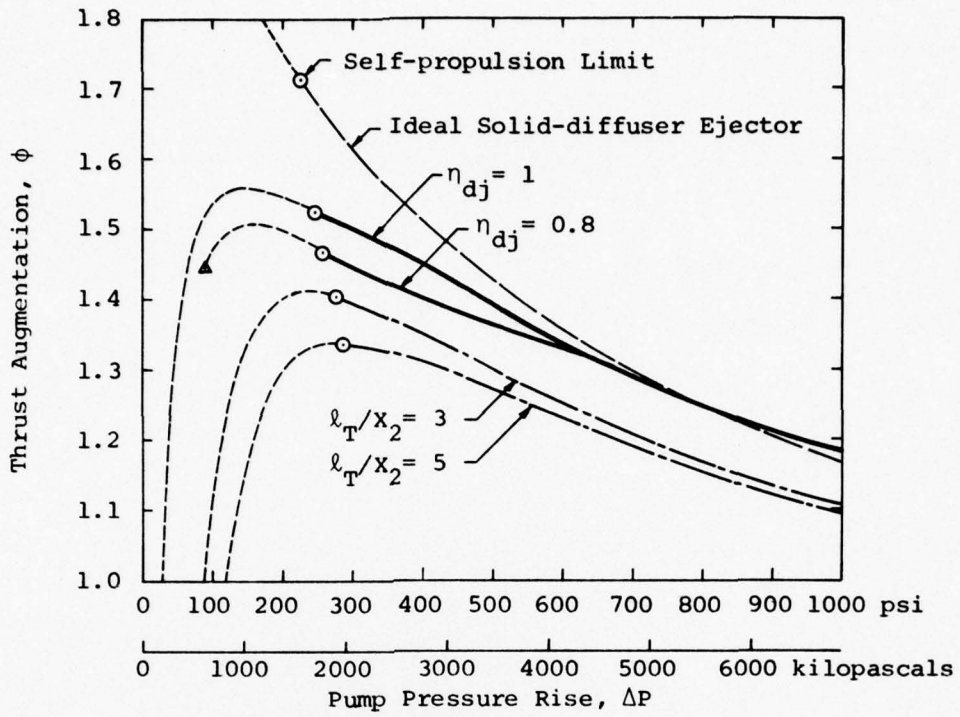

Condition: Non-cavitating; $U_\infty = U_p$ = 12.4 m/sec (24 knots); U_e/U_∞ = 0.5; Depth = 3.7 m (12 feet); $A_2/(s_\infty + a_\infty)$ = 40;

——— Ideal solid-diffuser ejector ($s_\infty = \dot{m}_d = 0$)

——— Solid-diffuser ejector ($s_\infty = \dot{m}_d = 0$) with ARL loss coefficients, η_N = 0.96; C_f = 0.0049; C_{di} = 0.025

——— Jet-diffuser ejector with losses, C_{di} = 0.01; C_{fdj} = fn(Re_ℓ); η_N = 1; $\dot{m}_d/\dot{m}_p$ = 0.2; Throat width = 10.2 cm (4 in.)

Figure 23. COMPARISON OF SOLID-DIFFUSER AND JET-DIFFUSER EJECTOR PERFORMANCE

VI CONCLUSIONS and REMARKS

The merits of ejector thrusters for application to marine vehicles can be evaluated correctly only if the ejector design and its power supply equipment are selected by an optimization procedure carried out under the prescribed operational conditions and in the light of other specific limitations which are associated with the system under consideration. This type of optimization must be carried out with a knowledge of the characteristics of the flow at the inlets to the ejector and the pump, and with realistic evaluations of the losses associated with the ejector. Care must also be exercised to take into consideration the performance limitations due to cavitation, self-propulsion (if required), and skin friction dissipation of the diffuser jet.

In general, high ejector performance requires large diffuser area ratios but the use of large diffuser area ratios results in long diffusers and the requirement for boundary layer control. High ejector performance also depends upon the achievement of rapid mixing of primary and induced flows. The achievement of rapid mixing can reduce the length requirement of ejector designs and reduce the loss due to skin friction, but is usually accompanied by increased inlet drag. Analytical results reported in this document suggest that an increase in the effective area ratio of the diffuser can compensate for incomplete mixing. Therefore the difficulty of achieving large diffuser area ratios is probably the key factor limiting the performance of stationary solid diffuser ejectors.

Although large diffuser area ratios are essential to the achievement of high thrust augmentation, the area ratio which can be utilized in an underwater environment is limited by cavitation. As the vehicle speed is increased, the maximum diffuser area ratio that can be utilized without cavitation at any given depth is decreased. Thus since small diffuser area ratios must be used for high speed vehicles, the loss due to separation is small and the performance of the ejector approaches that of an ideal ejector if skin friction and other loss factors can be minimized.

The performance/size advantage attributable to the use of a jet-diffuser results primarily from its capability to maintain flow attachment through a widely diverging solid diffuser and to the reduction of skin friction and separation losses when compared to a solid-diffuser of the same area ratio.

In addition, a jet-diffuser can achieve effective area ratios larger than the geometric area ratio of its solid surfaces in direct contrast to the solid diffuser whose effective area ratio is always smaller than the geometric area ratio.

To be effective, mixing of primary and induced flow must occur within the flow pattern where the static pressure is sub-ambient. Thus in a solid-diffuser ejector where the static pressure returns to ambient at or upstream of the end of the solid surfaces, the effective mixing process must occur within those surfaces. In a jet-diffuser the pressure remains sub-ambient for a considerable distance downstream of the solid surfaces and therefore this region is available for effective mixing. Thus the small size of a jet-diffuser does not limit the region available for effective mixing. Further, it has been demonstrated that in the event that mixing is not completed within the sub-ambient pressure region, a small increase in the effective diffuser area ratio can compensate for the performance degradation due to incomplete mixing. This increase in the effective diffuser area ratio is easily accomplished by a jet-diffuser.

Although an analysis of the propulsion system component sizes and weights was not attempted in this effort, several advantages are attributable to the ejector in comparison to the free jet or to a propeller. For example, the thrust augmentation relates the thrust achievable by an ejector system in comparison to the thrust of a free jet which utilizes identical power supply components. Obviously a thrust augmentation greater than 1.0 indicates that the ejector can produce thrust in excess of that of the free jet with identical machinery by the factor ϕ. In this regard it is important to note that the values of ϕ quoted in this document include all losses and are therefore realistic and achievable in an actual installation.

A different but very useful comparison of ejector thrusters with free jets is provided by the relative power (R_p). This parameter describes the ratio of power required to drive an ejector of specified geometry, operational and injected fluid characteristics, to the power required by a free jet which produces the same net thrust at the same pump flow rate and the same operational and injected fluid characteristics. Thus R_p less than 1.0 indicates that the ejector requires less power than does the corresponding free jet. The savings in fuel consumption is thus immediately discernible by a determination of the relative power. In practical ejector designs, the relative power (R_p) is closely proportional to $1/\phi^2$.

The relationship of machinery size and weight are also related to the power requirements but a precise estimate of these factors must also consider the optimal pump head and mass flow for each system. The optimal pump head for the ejector may be quite different from that for a free jet and therefore the machinery size and weight must be determined under optimal injected flow characteristics for each device.

Since ejectors do not require rotating components except possibly for their power supply which may be remote to the thrust producing element, it is feasible to contour the ejector to fit the shape of the vehicle being propelled. This can result in the ability to ingest boundary layer or wake fluid into the ejector with an accompanying increase in performance compared to that of an ejector which ingests free-stream fluid. The ability to ingest boundary layer fluid can also be utilized to control or remove the boundary layer and thereby reduce vehicle drag. Some examples of the performance benefit resulting from the ingestion of boundary layer fluid without regard to the drag reduction are presented in this document. In general the ingestion of boundary layer fluid reduces the ram drag and permits the use of larger diffuser area ratios without cavitation, thus resulting in larger thrust augmentation than is achievable by the same ejector ingesting free-stream fluid.

The work reported in this document forms a basis for design of ejector thrusters under virtually any set of requirements imposed by the vehicle system. Although some specific examples of the procedures for optimization are provided, it is essential that these procedures be repeated for any set of specifications if optimal performance and power supply selection is to be achieved. The possibility for avoiding the disadvantages of free jet propulsion and of propellers indicates the desirability of further investigation of the relative merits of ejectors vs other types of marine propulsion systems.

REFERENCES

1. Alperin, M., Wu, J. J. and Smith, Ch. A. "The Alperin Jet-Diffuser Ejector (AJDE) Development, Testing, and Performance Verification Report", Flight Dynamics Research Corporation, February 1976, NWC TP 5853.

2. Alperin, M. and Wu, J. J. "Underwater Ejector Propulsion, Theory and Applications", Flight Dynamics Research Corporation, October 1976, FDRC 0812-11-76.

3. Spence, D. A. "The Lift Coeffecient of a Thin Jet-Flapped Wing" Aero. Dep't., Royal Aircraft Establishment, Farnborough, Hants, Proc. Roy. Soc., A238, 1956.

4. Quinn, B. "Recent Developments in Large Area Ratio Thrust Augmentors", AIAA Paper No. 72-1174, AIAA/SAE 8th Joint Propulsion Specialist Conference, 1972.

5. Alperin, M. and Wu, J. J. "End Wall and Corner Flow Improvements of the Rectangular Alperin Jet-Diffuser Ejector", Flight Dynamics Research Corporation, May 1978, NADC-77050-30.

INITIAL DISTRIBUTION

	Number of Copies
Office of Naval Research	
800 North Quincy St.	
Arlington, VA 22217	
Attn: Power Program, K. Ellingsworth	5
Spec. Assist. Marine Corps Matters	2
Vehicle Systems Program, Code 221	1
Jim Smith, Code 431	1
R.F. Obrochta, Code 212	1
DDC	
Bldg. 5	
Cameron Station	
Alexandria, VA 22314	12
Naval Research Laboratory	
4555 Overlook Ave.	
Washington, D.C. 20390	
Attn: Tech. Info. Division	12
U.S. Naval Post Graduate School	
Monterey, CA 93940	
Attn: Dept. of Mechanical Engineering	1
Dept. of Aeronautics	1
U.S. Naval Academy	
Annapolis, MD 21402	
Attn: Dept. of Mechanical Engineering	1
Dept. of Aeronautics	1
ONR Branch Office	
1030 East Green St.	
Pasadena, CA 91106	
Attn: Mr. Ben Cagle	1
Naval Sea Systems Command	
Crystal City, NC #3	
Washington, D.C. 20360	
Attn: Chief Scientist, Code 03C	1
Marine Corps RDT&E Prog. Coord., Code 03M	2
Adv. Ship Devel. Br., Code 032	1
Amph. Assault Land. Craft, Code 032J	1
Underwater Weapon Propulsion, Code 0331	1
Ship Main Prop. & Energy, Code 0331	1
Hydromechanics, Code 0351	1
Undersea Warfare Systems Group, Code 06H	1
Submarine Directorate, Code 92	1
Naval Ship Engineering Center	
3700 East-West Highway	
Prince George Plaza	
Hyatsville, MD 20782	
Attn: Propulsion Sys. Analysis Br., Code 6144	2

Naval Ship R&D Center
Annapolis, MD 21402
Attn: Power Systems Division, Code 272 1
Gas Turbine Br., Code 2721 1

Naval Ship R&D Center
Carderock, MD 20034
Attn: Sys. Devel. Dept., Code 11 1
Ship Performance Dept., Code 15 1
Aviation & Surface Effects Dept., Code 16 1

Naval Underwater Systems Center
Newport, R.I. 02840
Attn: Energy Conversion Br., Code 36322 1

Naval Undersea Center
San Diego, CA 92132
Attn: Advanced Concepts Div. 1
Hydromechanics Div. 1

Naval Coastal Sys. Lab.
Panama City, FL 32401
Attn: Coastal Warfare Dept. 1

Naval Weapons Center
China Lake, CA 93555
Attn: Brad Kowalsky, Code 3183 2

Naval Surface Weapons Center
White Oak, MD 20910
Attn: Dr. C.Y. Zovko, Bldg. 308 1

Naval Air Systems Command
Jefferson Plaza
Washington, D.C. 20360
Attn: Propulsion Administrator, Code 330 1

Naval Air Propulsion Test Center
Trenton, N.J. 08628
Attn: Mr. Roman Dejneka 2

Defense Advanced Research Projects Agency
1400 Wilson Blvd.
Arlington, VA 22209
Attn: Dr. George Donahue 1

Maritime Administration
Commerce Bldg.
14th & E. Sts., NW
Washington, D.C.
Attn: Mr. Frank Critelli 1

Institute for Defense Analyses
400 Army Navy Dr.
Arlington, VA 22202
Attn: Dr. F.R. Riddell 1

U.S. Coast Guard
400 7th St. SW
Washington, D.C. 20590
Attn: Capt. D. Flannigan
G-DST/62 TR PT 1

Massachusetts Institute of Technology
77 Massachusetts Ave.
Cambridge, Mass. 02139
Attn: Prof. A.D. Carmichel
Dept. of Ocean Engineering 1

Carman Mazza
Flight Dynamics Branch
Air Vehicle Technology Department
NADC, Warminster, PA 18974 1

Dr. A.L. Slafkosky
Scientific Advisor
Commandant of the Marine Corps (Code RD-1)
Washington, D.C. 20380 1